Global Biogeochemical Cycles

RESEARCH ARTICLE
10.1029/2023GB008080

Special Collection:
Fjords: Estuaries on the Front-line of Climate Change

A Close Look at Dissolved Silica Dynamics in Disko Bay, West Greenland

Mark J. Hopwood[1], Dustin Carroll[2], Yuanyuan Gu[1], Xin Huang[1], Jana Krause[3], Stefano Cozzi[4], Carolina Cantoni[4], María Fernanda Gastelu Barcena[5], Shandy Carroll[6], and Arne Körtzinger[3]

[1]Department of Ocean Science and Engineering, Southern University of Science and Technology, Shenzhen, China, [2]Moss Landing Marine Laboratories, San José State University, Moss Landing, CA, USA, [3]GEOMAR Helmholtz Centre for Ocean Research Kiel, Kiel, Germany, [4]CNR-ISMAR Consiglio Nazionale delle Ricerche, Istituto di Scienze Marine, Trieste, Italy, [5]University of Florida, Gainesville, FL, USA, [6]County of Monterey, Monterey, CA, USA

Key Points:

- Both runoff and entrainment in subglacial discharge plumes influence estuarine nutrient dynamics around Disko Bay
- Entrainment from saline waters explains 93 ± 51% of dSi enrichment in the Ilulissat Icefjord outflow, freshwater <3%
- We estimate 0.25 and ∼1.9 Gmol yr^{-1} dSi fluxes from Greenland's icebergs and pelagic aSi dissolution, respectively

Supporting Information:

Supporting Information may be found in the online version of this article.

Correspondence to:

M. J. Hopwood,
mark@sustech.edu.cn

Citation:

Hopwood, M. J., Carroll, D., Gu, Y., Huang, X., Krause, J., Cozzi, S., et al. (2025). A close look at dissolved silica dynamics in Disko Bay, west Greenland. *Global Biogeochemical Cycles*, *39*, e2023GB008080. https://doi.org/10.1029/2023GB008080

Received 14 DEC 2023
Accepted 13 DEC 2024

Author Contributions:

Conceptualization: Mark J. Hopwood, Dustin Carroll, Jana Krause
Data curation: Mark J. Hopwood, Yuanyuan Gu, Jana Krause, Stefano Cozzi
Formal analysis: Mark J. Hopwood, Yuanyuan Gu, Xin Huang, Stefano Cozzi, Carolina Cantoni, María Fernanda Gastelu Barcena, Arne Körtzinger
Funding acquisition: Mark J. Hopwood, Dustin Carroll

Abstract Discharge of calved ice, runoff and mixing driven by subglacial discharge plumes likely have consequences for marine biogeochemistry in Disko Bay, which hosts the largest glacier in the northern hemisphere, Sermeq Kujalleq. Glacier retreat and increasing runoff may impact the marine silica cycle because glaciers deliver elevated concentrations of dissolved silica (dSi) compared to other macronutrients. However, the annual flux of dSi delivered to the ocean from the Greenland Ice Sheet is poorly constrained because of difficulties distinguishing the overlapping influence of different dSi sources. Here we constrain silica dynamics around Disko Bay, including the Ilulissat Icefjord and four other regions receiving glacier runoff with contrasting levels of productivity and turbidity. Both dissolved silica and Si* ([dSi]-[NO_x^-]) concentrations indicated conservative dynamics in two fjords with runoff from land-terminating glaciers, consistent with the results of mixing experiments. In three fjords with marine-terminating glaciers, macronutrient-salinity distributions were strongly affected by entrainment of nutrients in subglacial discharge plumes. Entrainment of dSi from saline waters explained 93 ± 51% of the dSi enrichment in the outflowing plume from Ilulissat Icefjord, whereas the direct contribution of freshwater to dSi in the plume was likely 0%–3%. Whilst not distinguished herein, other minor regional dSi sources include icebergs and dissolution of amorphous silica (aSi) in either pelagic or benthic environments. Our results suggest that runoff around Greenland is supplemented as a dSi source by minor fluxes of 0.25 ± 0.67 Gmol yr^{-1} dSi from icebergs and ∼1.9 Gmol $year^{-1}$ from pelagic aSi dissolution.

Plain Language Summary Silica is one nutrient required by marine phytoplankton, specifically siliceous microalgae such as diatoms. Glacier runoff delivers higher concentrations of silica into the ocean compared to other nutrients such as nitrate or phosphate. Changes in the cryosphere, such as glacier retreat and increasing ice discharge or runoff, may therefore have downstream ecological effects due to shifts in the availability, and ratios, of nutrients. However, the magnitude of dissolved silica fluxes into the ocean from the present day Greenland Ice Sheet has proven challenging to determine, with two existing estimates varying by an order of magnitude. This is because of uncertainties in how to disentangle the overlapping influence of different dSi sources. Here, we conducted a detailed survey of the Disko Bay region in west Greenland, including inshore and offshore dSi measurements, to assess how the chemistry of dSi changes in estuaries. In order to further understand estuarine dSi dynamics, we conducted incubation experiments at sea and in the laboratory. Our results reduce uncertainty in the magnitude of dSi supplied to the ocean from Greenland's glaciers and suggest a modest dSi flux from runoff with small additional fluxes from melting icebergs and dSi release from suspended particles.

1. Introduction

Silica is an essential macronutrient for siliceous microalgae and thus a key driver of phytoplankton bloom dynamics (Armbrust, 2009; Brzezinski, 1985; Tréguer & De La Rocha, 2013). In the Arctic, diatoms typically deplete dissolved silica (dSi) prior to nitrate (NO_3^-) leading to dSi limitation of diatom growth (Krause et al., 2018, 2019). In glacier fjords, the ratio of dSi:NO_3^- is affected by discharge from glaciers because runoff is deficient in nitrate and phosphate relative to dSi (Cape et al., 2018; Kanna et al., 2018; Meire et al., 2016). The latest global marine budget for dSi suggests that ice sheets are a major dSi source to the global ocean (Tréguer et al., 2021), estimated to deliver 0.3 Tmol dSi yr^{-1}. Recent increases in the annual fluxes of runoff and calved ice

Investigation: Mark J. Hopwood, Dustin Carroll, Xin Huang, Stefano Cozzi, Carolina Cantoni, María Fernanda Gastelu Barcena, Shandy Carroll, Arne Körtzinger
Methodology: Mark J. Hopwood, Yuanyuan Gu, María Fernanda Gastelu Barcena
Project administration: Mark J. Hopwood, Jana Krause
Resources: Mark J. Hopwood, María Fernanda Gastelu Barcena, Arne Körtzinger
Supervision: Mark J. Hopwood, Arne Körtzinger
Writing – original draft: Mark J. Hopwood, Dustin Carroll
Writing – review & editing: Mark J. Hopwood, Dustin Carroll, Yuanyuan Gu, Xin Huang, Jana Krause, Stefano Cozzi, Carolina Cantoni, María Fernanda Gastelu Barcena, Shandy Carroll, Arne Körtzinger

from Greenland (Mankoff, Noël, et al., 2020; Mankoff, Solgaard, et al., 2020) might therefore affect the regional dSi budget on annual timescales (Hawkings et al., 2017; Krause et al., 2019). A high budget component of dSi from the Greenland Ice Sheet however is in disagreement with observed dSi concentrations from the Greenland shelf (Boyer et al., 2018). Profiles of all macronutrients show that glacier fjords are almost universally macronutrient sinks because they are characterized by an inflow of saline and macronutrient-rich waters at depth, and an outflow of fresher and macronutrient-deficient waters nearer the surface (e.g., Cape et al., 2018; Holding et al., 2019; Kanna et al., 2018; Meire et al., 2017; Seifert et al., 2019). This might explain why dSi anomalies have not yet been detected on the Greenland shelf in years with high freshwater discharge (Tesdal et al., 2022) and why regional models for Disko Bay match observed dSi concentrations reasonably well without including a specific dSi source from glaciers (Møller et al., 2023).

Glacier-associated sources of dSi can be broadly divided into the direct dSi addition from runoff, ice-melt, and groundwater (Meire et al., 2016; Yde et al., 2014); the net-release of dSi from amorphous Si (aSi) phases in suspension prior to their deposition in marine-sediments (Hawkings et al., 2017); and the net-release of dSi from marine sediments (Ng et al., 2020). Some of these sources are better constrained than others. Dissolved Si concentrations in runoff have been measured at numerous sites around Greenland, suggesting an average concentration of 22–27 μM dSi using data from the best studied catchments in west Greenland (Andrews et al., 2018; Graly et al., 2017; Hatton et al., 2019; Martin et al., 2020; Meire et al., 2016; Yde et al., 2005). Icebergs likely contain lower dSi concentrations with a less well constrained average (but likely less than <10 μM) (Meire et al., 2016). Groundwater dSi fluxes are not constrained and, whilst groundwater is thought to be a minor budget term for freshwater discharge (DeFoor et al., 2011), the dSi concentration associated with this source may be higher than runoff. Benthic dSi effluxes have been mainly derived on the southwest Greenland shelf and in Nuup Kangerlua (southwest Greenland) ranging from 0.3 to 3 mmol m^{-2} day^{-1} (Ng et al., 2020).

Amorphous silica concentrations, which can be sourced from glacier weathering processes, are high in sediments and soils around Greenland (Alfredsson et al., 2016; Stimmler et al., 2023) and certainly present in runoff at higher concentrations than dSi with an estimated mean concentration of 392 μM (Hawkings et al., 2017). Glacier-derived aSi dissolution is quantitatively converted to dSi in budgets that explicitly include it (Hawkings et al., 2017; Tréguer et al., 2021) leading to a global glacier-to-ocean dSi flux estimate of 0.3 Tmol $year^{-1}$, ~95% of which is from aSi dissolution in the ocean (Hawkings et al., 2017). This is assumed to be additional to the measured dSi fluxes from runoff and icebergs. The single largest component of the annual delivery of dSi to the ocean from the Greenland Ice Sheet has therefore been argued to be the dissolution of aSi in seawater, accounting for an order of magnitude higher dSi input than directly arises from runoff dSi additions. Yet it is unclear if aSi-derived dSi fluxes are strictly additive because the supply of dSi from aSi dissolution may already be incorporated in budgets depending on exactly when and where aSi dissolution occurs.

The strongest evidence for a large additive budget component of aSi dissolution to dSi inventories around Greenland is an unusual dSi-salinity trend in Kangerlussuaq (west Greenland), which is argued to result from aSi release driving strong non-conservative dSi dynamics (Hawkings et al., 2017). This would require aSi dissolution rates faster than those measured to date (Hatton et al., 2023; Hawkings et al., 2017). However, this trend is not evident in other limited data sets from Kangerlussuaq (Lund-Hansen et al., 2018) or other glacier-fjords around Greenland (Holding et al., 2019; Kanna et al., 2018; Krause et al., 2021; Krisch et al., 2021; Meire et al., 2017; Seifert et al., 2019). One potential explanation for this is that the rapid release of dSi could be counteracted by strong drawdown by diatoms on a similar spatial scale. Isotopic dSi data from Nuup Kangerlua (southwest Greenland) have been suggested to support this hypothesis (Hatton et al., 2023), implying that a boundary exchange of dSi imparts a glacier-associated signal in dSi isotopes in a glacier fjord without leading to evidence of strong non-conservative addition in the dSi-salinity relationship. If this process were to act on a large scale, it could potentially explain why Greenland's fjords largely remain a net-nutrient sink despite accounting for a significant calculated fraction of the global annual dSi outflow to the ocean. This hypothesis should also be easy to test as, if it were correct, a strong divergence should be observed between the (non-)conservative nature of dSi in high- and low-productivity glaciated estuaries.

A further critical key question is how to incorporate any aSi dissolution into flux estimates. Amorphous Si dissolution may not only occur in marine pelagic environments. A degree of aSi dissolution has likely already occurred in runoff when freshwater enters the ocean. When dSi concentrations in runoff are measured close to the coastline (as herein), the aSi dissolution occurring in runoff is included in runoff dSi fluxes. If aSi dissolution

continues to occur in surface glacially modified fjord waters, any released dSi would be included in runoff flux estimates derived using estuarine mixing diagrams for low-productivity environments where diatom dSi drawdown was insignificant. However, amorphous Si may have only a short residence time in the surface layer- if it enters the surface layer at all, as particles delivered from marine-terminating glaciers may remain at depth (e.g., Azetsu-Scott & Syvitski, 1999; Cape et al., 2018; Krisch et al., 2021). The dissolution of aSi may accordingly also occur in deep, saline water layers. Furthermore, after aSi is deposited in fjord, or shelf, sediments, net effluxes of dSi into the water column likely include some degree of aSi dissolution (Ng et al., 2020). In these cases, any resulting dSi additions to the water column would be largely decoupled in space and time from freshwater inputs. Turbidity from glacier discharge plumes is generally attenuated strongly at spatial scales of ∼10 km from glaciers (Azetsu-Scott & Syvitski, 1999; Kanna et al., 2018; Mugford & Dowdeswell, 2011) such that fjord surveys often do not measure the most turbid, potentially aSi-rich, waters emerging from land- or marine-terminating glaciers. Concurrently, sediment accumulation rates decline exponentially downstream of Greenland's glaciers in all measured case studies (Andresen et al., 2024). A large fraction of the aSi released in meltwater might therefore be expected to be deposited within fjord systems close to glacier outflows, potentially concentrating the release of dSi from aSi in benthic systems. Most of Greenland's studied fjords, including the Ilulissat Icefjord (Gladish et al., 2015), overturn relatively rapidly, with the deep saline waters renewed within ∼1 month or less (Slater et al., 2022). Thus, any aSi dissolution occurring in deep fjord waters may not be evident as strongly enriched dSi concentrations because of the large volume of deep fjord layers. However, any released dSi should be included within vertical flux calculations derived using in-fjord dSi profiles and accordingly may contribute to the dSi available to support diatom growth within the same season (Meire et al., 2016).

Disko Bay hosts several distinct glacier outflows, including the largest glacier by annual discharge and calved ice volume in the northern hemisphere, Sermeq Kujalleq (otherwise known as Jakobshavn Isbræ; Mankoff, Solgaard, et al., 2020). Sermeq Kujalleq releases large icebergs and subglacial discharge into the Ilulissat Icefjord, which retains a cover of dense ice mélange throughout most of the year. This is largely because of a 50–245 m deep sill at the fjord mouth, which restricts the export of large icebergs (Gladish et al., 2015). Dense ice cover and the UNESCO Natural World Heritage Site status of the Icefjord mean that it is a relatively poorly surveyed glacier-fjord system. Discharge from Sermeq Kujalleq may however have profound effects on coastal productivity (Møller et al., 2023). Satellite derived chlorophyll data suggest that this is one of the only glacier systems around Greenland large enough to affect coastal plankton dynamics, with increasing summertime chlorophyll since the 1990s observed in parallel with increasing discharge (Oliver et al., 2023). This aligns well with theory, which predicts that a large buoyant meltwater plume from Sermeq Kujalleq (Gladish et al., 2015; Slater et al., 2022) generates a significant vertical flux of entrained macronutrients throughout summer (Cape et al., 2018). In addition to Sermeq Kujalleq, relatively large glaciers including Saqqarliup Sermia, Eqip Sermia, Sermeq Kujatdieq, and Sermeq Avangnardleq terminate in fjords that surround Disko Bay.

Sermeq Kujalleq and the Ilulissat Icefjord are unusual compared to many other Greenlandic glacier fjord systems in terms of the large magnitude of freshwater discharge (Mankoff, Noël, et al., 2020) and the ice-covered nature of the fjord surface in summer. Yet, these features may be particularly insightful for studying the processes by which nutrients are cycled downstream of glacier outflows. Other large marine-terminating glacier fjords studied around Greenland to date including, for example, Sermilik, Nuup Kangerlua and Bowdoin, have several common features (Hopwood et al., 2020). During the meltwater season, these fjords exhibit entrained macronutrient plumes which emerge from the glacier grounding line depth and drive anomalously high macronutrient concentrations in the upper water column (Cape et al., 2018; Kanna et al., 2018; Meire et al., 2017). The depth of these features vary between fjords, and years (De Andrés et al., 2020), and can be found from close to the surface down to ∼200 m depth depending on factors including the rate of freshwater discharge and ambient stratification (Cape et al., 2018; Kanna et al., 2018; Meire et al., 2017). Inner-fjord turbid environments are generally low productivity environments, but moving down-fjord plankton blooms driven by entrained plumes are observed typically at around 20–40 m depth (Kanna et al., 2022; Meire et al., 2017). This results in the drawdown of macronutrients in the outflowing surface layer such that fjord outflow is often nutrient deficient compared to fjord inflow at depth (Juul-Pedersen et al., 2015; Kanna et al., 2018). To quantify the impact of these features on dSi fluxes, we define two key flux gates (Figure 1). The first is the vertical flux of nutrients entrained in a buoyant plume close to the glacier face (Jenkins, 2011; Slater et al., 2022). In an idealized two box model of a large glacier fjord, this vertical flux (Flux Gate A, Figure 1) represents the main mechanism via which nutrients are transported from deep to surface waters in summer and thus able to support plankton blooms (Carroll et al., 2017; Meire et al., 2017; Oliver

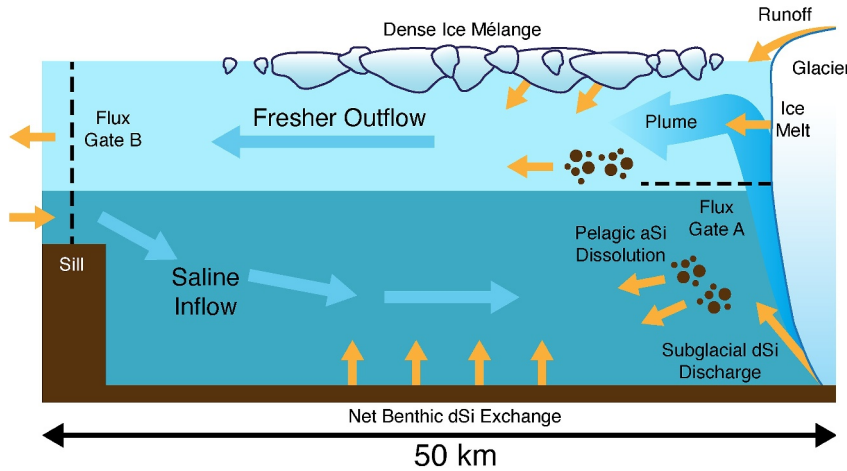

Figure 1. Conceptual along-fjord section for the Ilullisat Icefjord. Water movements are illustrated in blue and dSi fluxes are annotated in yellow. Two flux gates are defined. Flux Gate A corresponds to the "upwelled" or "entrained" nutrient flux associated with the vertical flux of nutrients in a subglacial discharge plume. Flux Gate B corresponds to the net outflow from the fjord over the sill.

et al., 2020). This flux, referred to in prior work as the upwelled or entrained nutrient flux, has been found to explain observed nitrate concentrations in multiple case-studies around Greenland (Cape et al., 2018; Hopwood et al., 2018; Oliver et al., 2023) and also constitutes an important component of in-fjord dSi budgets (Meire et al., 2016). Where this vertical flux is deduced from fjord water column profiles (e.g., Meire et al., 2016), it represents the vertical transport of dSi into the surface layer irrespective of its origin (i.e., whether from saline inflow to the fjord, dissolution within the fjord water column, or benthic effluxes). We define a second flux gate at the fjord mouth (Flux Gate B, Figure 1). At the fjord mouth, Greenland's fjords are usually characterized by an inflow of saline, nutrient-rich waters at depth and an outflow of fresher, nutrient-deficient waters in a glacially modified surface layer (Kanna et al., 2018; Meire et al., 2017; Straneo & Cenedese, 2015). The difference between inflowing and outflowing water masses constrains the net effect of all processes that occur within the fjord, which in summertime includes the drawdown of dSi by diatom blooms (Krawczyk, Arendt et al., 2015; Krawczyk, Witkowski et al., 2015; Krawczyk et al., 2014). However, here the Ilulissat Icefjord is critically different from other large systems (e.g., Nuup Kangerlua, Sermilik and Bowdoin) because of dense thick ice mélange which extends >50 km from the calving front to the sill throughout summer (Figure 1). Despite the relatively shallow depth of the outflowing glacially modified layer in the upper ~170 m of the Icefjord, with the fastest outflow at 20 m depth (Gladish et al., 2015), prior work suggests that nutrients exit the Icefjord at the fjord mouth without having experienced much drawdown (Cape et al., 2018). Accordingly, the Icefjord is an interesting system in which to construct nutrient budgets in order to attempt to explain the magnitude of nutrient anomalies at the fjord mouth.

In order to bridge inshore and offshore based studies of dSi dynamics around Greenland and to reduce uncertainty in dSi budgets, we combined a research cruise in Disko Bay ("GLICE") with an inshore pre-cruise campaign in Ilulissat and Saqqarleq Fjord ("Ice Disko") to study the trends in dSi over the glacier-ocean continuum. We combined a survey of macronutrients (nitrate, phosphate and dSi) with mixing and incubation experiments to test the short-term response of seawater dSi dynamics to plumes of glacier rock flour.

2. Materials and Methods

2.1. Field Sampling

A short field campaign was conducted during 5–9 August 2022 to sample close to the ice mélange edge in the mouth of Ilulissat Icefjord (box 3, Figure 2); mid-Icefjord at the junction with Saqqarleq Fjord, which has open water throughout summer (box 3, Figure 2); and in the southern part of Saqqarleq Fjord close to the marine-terminating glacier Saqqarliup Sermia (box 4, Figure 2). 14 CTD casts were deployed down to 40 m from small fishing boats with GO-FLO bottles deployed at five stations on a nylon line. Additional surface samples

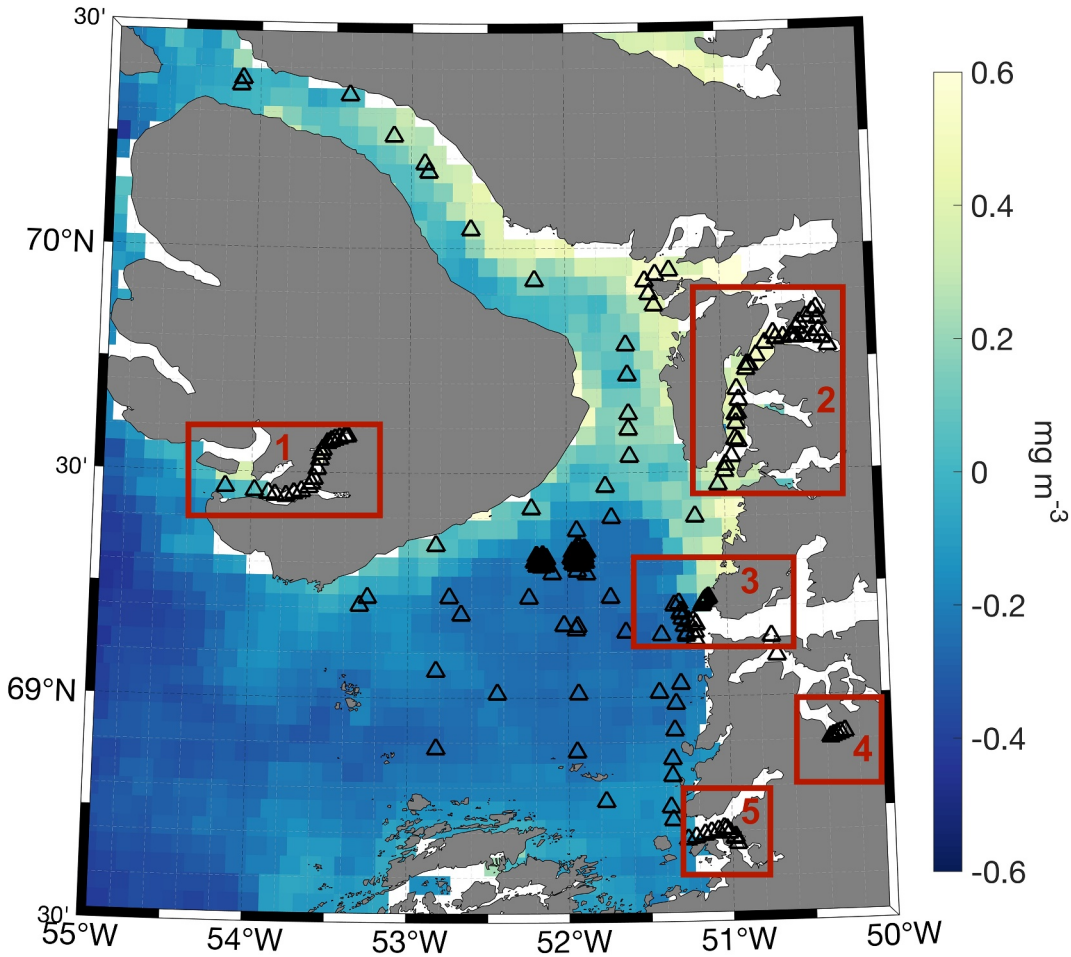

Figure 2. Satellite-derived chlorophyll data for Disko Bay. August 2022 monthly mean chlorophyll annotated with the locations of surface samples from either underway measurements or profiles. Five surveyed areas with large glacier outflows are annotated with boxes: (1) Disko Fjord, (2) Atâ Sund and the approach to Eqip Sermia, (3) Ilulissat Icefjord, (4) Saqqarleq Fjord and the approach to Saqqarliup Sermia, and (5) Kangersuneq. For a closer view of fjord sites, the reader is referred to Figure S2 in Supporting Information S1.

were collected by hand. Sampling, data and analysis protocols were as per the subsequent cruise (see below). For convenience, profiles from the pre-cruise campaign and the RV Sanna cruise are numbered sequentially. Runoff samples (zero salinity) were collected at 3 locations for incubation experiments: in Kangerlussuaq (67.0178°N, 50.6597°W), on the southwest bank of Saqqarleq Fjord (68.7607°N, 50.3191°W) and on the southeast bank of Saqqarleq Fjord (68.8295°N, 50.2757°W). Suspended particles were retained from the same sites by filtering 75–100 mL of water (0.2 μm polyethersulfone 47 mm filters, Sartorius) with the exact volume recorded. Wet bulk glacier flour samples were also retained from the same sites from sediment close to the river banks. Filters were frozen (−20°C) and four bulk glacier samples were refrigerated (4°C) until analysis.

RV Sanna (EUROFLEETS+ cruise GLICE) was deployed out of Ilulissat 10–23 August 2022. A SBE 911plus CTD (Sea-Bird Scientific, USA) was deployed from the ship's A-frame to conduct 126 depth profiles for CTD data, on 34 of which we also deployed GO-FLO samplers for water samples. A 60 kg steel towfish was deployed approximately 2 m away from the ship at 1–2 m depth while the ship cruised at 6–7 knots. Water was pumped from the towfish into an insulated sensor box on the deck with a calculated water residence time of ~8 min. Two separate sub-lines of the underway pump allowed direct sampling of underway water (one of which was trace metal clean using a separate Teflon diaphragm pump; DM15, Dellmeco, Germany). An EXO1 (YSI, USA) Water Quality Sonde equipped with salinity, temperature, turbidity and chlorophyll sensors was mounted in the insulated sensor box with data logged at intervals of 2 min or less throughout the cruise. Note that turbidity data

suffered some interference due to the slow flushing of particles after the ship entered turbid plumes with high particle loads (see Figure S1 in Supporting Information S1). CTD casts were deployed in a grid around the Bay area at ~10 km intervals down to ~100 m depth. Additional profiles were conducted close to the ice mélange edge in the mouth of the Icefjord (box 3, Figure 2) and in Atâ Sund along the approach to the glacier Eqip Sermia (box 2, Figure 2). At 11 locations with high visible turbidity, 1–2.5 L of surface water was filtered (0.2 µm polyethersulfone 47 mm filters, Sartorius) to retain suspended particles with the exact volume recorded.

2.2. Sample Analysis

Macronutrient data refers to frozen samples which were syringe filtered (Millipore 0.2 µm, polyvinyldifluoride) or filtered in line for towfish samples (AcroPak, 0.8/0.2 µm, polysulfone), stored at −20°C and shipped back to GEOMAR for analysis. Analysis of macronutrients was conducted for nitrate (NO_3^-), nitrite (NO_2^-), phosphate (PO_4^{3-}) and dSi by segmented flow injection analysis using a QUAATRO (Seal Analytical) auto-analyzer (Hansen & Koroleff, 1999). Recoveries of a certified reference solution (KANSO, Japan) were 98.0 ± 0.8% NO_x^-, 99.4 ± 1.4% PO_4^{3-} and 95.4 ± 8.1% dSi. Detection limits were 0.019 µM NO_x^-, 0.002 µM NO_2^-, 0.027 µM PO_4^{3-}, and 0.033 µM dSi. NO_2^- was close to the detection limit throughout the data set and so we generally refer to NO_x^- which was practically interchangeable with NO_3^- ($[NO_x^-] = 1.00 \times [NO_3^-]$, $R^2 = 1.00$). Si* was calculated as [dSi]-[NO_x^-].

Amorphous Si concentrations were determined on suspended particles retained from runoff and surface fjord water, and on bulk glacier flour samples retained from the river banks adjacent to where suspended particles were collected. In all cases, sediment was handled wet as collected and separate subsamples were dried to constant mass to determine particle load. Amorphous Si was determined as per DeMaster (1981). For suspended particles, filter fractions corresponding to ~50 mg wet sediment were added to 40 mL of 0.096 M Na_2CO_3 solution maintained at 85°C in a water bath. For bulk glacier flour samples, a higher sediment load of 200 mg was used due to the lower aSi concentrations in coarser aged material compared to finer suspended particles. At 1, 2, 3, and 5 hr, 2 ml sample aliquots were extracted. All aliquots were then adjusted to pH 8 via the addition of a 0.04 HCl solution, and dSi was analyzed using the batch molybdenum blue method (Grasshoff et al., 1983). Linear regression of dSi concentration versus sample collection time was then obtained, with the intercept interpreted as aSi. This assumes that aSi phases are dissolved completely within the first hour of extraction while more crystalline Si phases are released at a constant rate.

2.3. Mixing and Seawater Incubation Experiments

Three mixing experiments were conducted at sea between filtered seawater and unfiltered glacier runoff to assess the possibility of rapid changes in dSi concentration across the salinity gradient. Runoff naturally laden with glacier rock flour from three sites (one in Kangerlussuaq and two in Saqqarleq Fjord) was retained and refrigerated in the dark. A macronutrient sample was filtered and retained both on the day of collection and on the day when the mixing experiment was set up. Coastal seawater (S = 31.5 psu) was collected from 10 m depth at a coastal station with low turbidity and lower dSi than in-fjord stations (CTD station 71; 69.136° N, 51.258° W) and filtered to remove any suspended particles (0.8/0.2 µm AcroPak, polyethersulfone). Low-density polyethylene incubation bottles were rinsed once with filtered seawater, filled with 8 different mixtures ranging from 100% runoff to 100% seawater and then incubated in the dark at 6°C for 48 hr using a neutrally buoyant box suspended in a tank of seawater on deck with constant in/outflow. The exact mixing ratios were determined by mass; the eight mixed salinities were approximately 0, 5, 9, 16, 26, 29, 30, and 31. After 48 hr, macronutrient samples were collected and syringe filtered.

Upon return to the laboratory, further incubation experiments were conducted in an incubator (TS-2102GZ, Jintan Kingda Manufacturing) to assess the rate of aSi release from suspended particles in seawater. Coastal seawater was collected from Dapeng (22.5536°N, 114.5193°E) and allowed to stand in the dark for >3 months prior to starting the experiments. All experiments were conducted in the dark at 40 rpm using 1 L high density polyethylene bottles. Incubation bottles were filled with 600 mL seawater (salinity 33.3 psu). 400 mL headspace and caps with holes were used to facilitate air exchange and minimize changes to the carbonate system. Bottles were always incubated for one day prior to particle addition. Stream bed glacier rock flour from Kangerlussuaq was suspended at 10, 50, and 100 mg L^{-1} at 15°C with duplicate bottles prepared. A bottle was removed for sampling at time zero (when particles were added) and 1, 2, 3, 5, 10, and 21 days later. Suspended sediment from

Kangerlussuaq and two locations in Saqqarleq Fjord (all retained on filters) was incubated at 15°C with a sediment load of ~50 mg L^{-1} using the same setup. Filters used to collect suspended particles were subdivided and 1/8 fragments were added to each bottle. To assist the re-suspension of particles from filters, 10 mL seawater was used to re-suspended particles before addition to the 1 L bottles. A bottle was removed from the incubator for sampling at time zero and 3, 8, 13, and 28 days later. A replicate filter collected from the same sampling site was used to determine the initial aSi for these experiments. Note that due to the need to split filters holding suspended particles into multiple bottles, a compromise had to be made between replicating treatments or running more timepoints. As samples from 3 different locations were available, we opted to run the experiment as a timeseries without replication of each site (although the time zero value could be considered a triplicate measurement from 3 separate bottles).

2.4. Deriving a dSi Budget for Ilulissat Icefjord

To define the dSi outflow from the Ilulissat Icefjord (Flux Gate B, Figure 1), we conducted a series of profiles to 100 m depth across the fjord mouth at the ice mélange edge (Figure 2, box 3). These were verified to capture positive nutrient concentration anomalies in the upper 60 m compared to background profiles in Disko Bay (Figure S5 in Supporting Information S1). In the absence of sustained observations in the fjord mouth, fjord inflow was defined as per Gladish et al. (2015), noting that the inflowing density of saline waters entering the Icefjord for the 3 decades prior to 2014 was confined to the range σ_θ 27.2–27.3 kg m^{-3}. The properties of meltwater entering the fjord were defined using iceberg meltwater to represent a low dSi freshwater endmember and runoff from the Saqqarleq side-branch to define a high freshwater dSi endmember. The difference in the dSi: nitrate ratio contrasting inflow and outflow was then assumed to reflect net dSi sources within the Icefjord (see Methods 1 in Supporting Information S1 for an assessment of uncertainties associated with this comparison and Methods 2 in Supporting Information S1 for a comparison to a dSi budget derived for the best studied glacier fjord system in Greenland, Nuup Kangerlua).

3. Data

Monthly level 3 gridded chlorophyll *a* concentrations from January 2018 to July 2023 with a resolution of 4 km were obtained from the European Space Agency (ESA) Ocean Color Climate Change Initiative (OC-CCI) (Sathyendranath et al., 2019). Monthly sea surface temperature for August 2022 was obtained from the Moderate Resolution Imaging Spectroradiometer (MODIS-Aqua, Kilpatrick et al., 2015). Sea surface salinity at a resolution of 0.25° for August 2022 was obtained from the Multi Observation Global Ocean Sea Surface Salinity and Sea Surface Density (MULTIOBS) data set, which combines satellite and in situ salinity measurements and is available from Copernicus Marine Service (Droghei et al., 2016, 2018).

Data sets from fieldwork are available online from SeaDataNet. The following data sets report data discussed herein: GLICE Bottle biogeochemistry, GLICE Freshwater biogeochemistry, and GLICE CTD profiles (https://evior.eurofleets.eu/cds-report/17, last accessed 29.05.2024). SeaDataNet quality control flags were assigned to all core data. Sensor data were processed prior to submission to remove time periods when the ship was stationary and pumps were disengaged or when other routine maintenance issues were being resolved. For calculation purposes herein, values reported below the limit of detection were assigned a value of zero. Prior open access profiles for CTD and nutrient data in Disko Bay were collated as per the compilation by Slater et al. (2022) for summer (June to September).

4. Results and Discussion

4.1. Spatial Trends

Five inshore areas receiving glacier discharge had varying salinity, temperature, chlorophyll and turbidity relationships. Chlorophyll, both from underway sensor and satellite derived data (for August 2022), was highest in Atâ Sund and the approach to Eqip Sermia (box 2, Figure 2 and Figure S2 in Supporting Information S1). Intermediate levels were observed in Saqqarleq Fjord (box 4, Figure 2), and low values were observed at the mouth of Ilulissat Icefjord (box 3, Figure 2), in Disko Fjord (box 1, Figure 2) and in Kangersuneq (box 5, Figure 2). Salinity trends verified that all five sites exhibited a plume of low salinity meltwater (Figure 3). For Eqip Sermia and Ilulissat Icefjord, these plumes were cold with surface temperatures often <2°C, and occasionally <0°C for the Ilulissat Icefjord, likely due to the local influence of melting ice. Conversely, surface waters in Saqqarleq

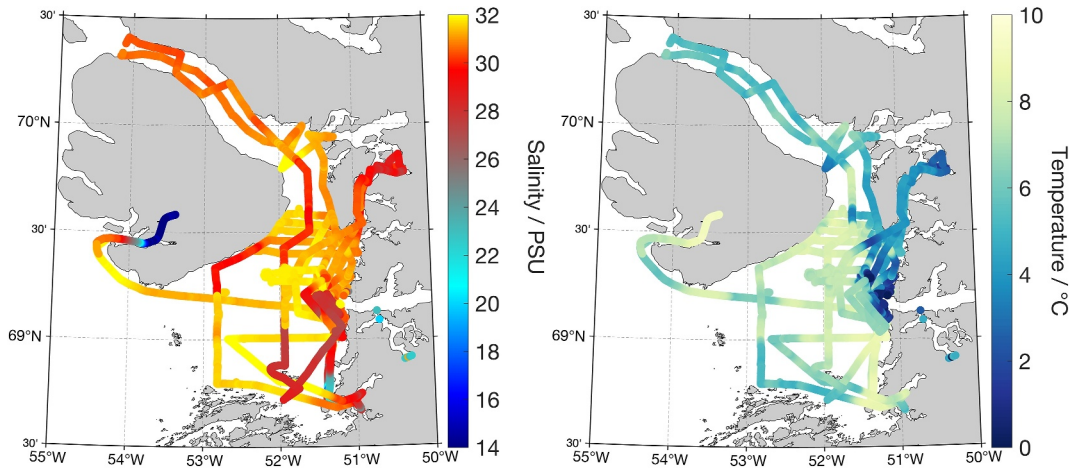

Figure 3. Underway properties along the cruise track from sensors deployed in the flow-through box. Near surface salinity (left) and temperature (right) assessed at 1–2 m depth at 2-min intervals. Additional spot measurements from the pre-cruise campaign in Ilulissat and Saqqarleq Fjord are also shown. A comparison to satellite derived sea surface salinity and temperature is shown in Figure S3 in Supporting Information S1.

Fjord, Kangersuneq and Disko Fjord were much warmer with temperatures up to 9°C (Figure 3). Turbidity levels were similarly high in Kangersuneq and Disko Fjord, lowest at the mouth of the Ilulissat Icefjord and intermediate for the other sites (Figure S1 in Supporting Information S1) (Note that turbidity trends are unreliable on cruise legs leaving areas with turbid plumes due to a lag of particles washing through the sensor box). These trends generally mirrored those previously observed in other glacier fjord systems in Greenland. Higher temperatures and turbidity, and lower chlorophyll concentrations are typically associated with low salinity plumes from runoff (Holding et al., 2019; Lund-Hansen et al., 2018; Stuart-Lee et al., 2023), whereas lower temperatures and turbidity, and higher chlorophyll concentrations are normally associated with subglacial discharge plumes from marine-terminating glaciers (Cape et al., 2018; Kanna et al., 2018; Meire et al., 2017).

Macronutrient concentrations were determined for 342 datapoints across Disko Bay (Figure 4). The highest dSi concentrations were found in Saqqarliup Sermia runoff (24.9 μM), in runoff from a proglacial river close to Eqip Sermia (30.9–32.0 μM), and in Disko Fjord (up to 47.9 μM at salinity 10.6 psu). Lower dSi concentrations were found in Kangersuneq, Eqip Sermia, Saqqarleq Fjord, and Ilulissat Icefjord (extrapolated freshwater endmembers were 9.4, 17.4, 11.8, and 24.3 μM dSi*, respectively). In the latter three cases, relatively low extrapolated dSi endmembers may reflect the influence of a large component of iceberg melt as a freshwater endmember component. Iceberg fragments analyzed for macronutrient content across the cruise area had a consistently low dSi concentration (mean 0.11 ± 0.41 μM, $n = 90$, Krause et al., 2024). This was much lower than the concentrations reported in runoff and at the low end of previous estimates of iceberg dSi concentration (Hawkings et al., 2017; Meire et al., 2016). Most of Disko Bay was characterized by high salinity waters with low dSi concentrations at the surface, although only five datapoints were below detection (<0.03 μM dSi). For salinity >31.2 psu, the surface dSi concentrations were always <1 μM.

4.2. Silica Distribution in Estuaries

Various salinity-dSi relationships were observed in the five different fjord regions sampled (Figure 4). The two systems with a few sources of runoff and no marine-terminating glacier influence showed approximately linear dSi-salinity relationships along the surface low-salinity plumes (Kangersuneq $R^2 = 0.76$, Figure 2 (box 5); and Disko Fjord $R^2 = 0.93$, Figure 2 (box 1)), with intercepts at zero salinity of 35 μM dSi for Kangersuneq and 68 μM dSi for Disko Fjord. A similar, but less linear, trend was observed for PO_4^{3-} in these two catchments (Kangersuneq $R^2 = 0.13$ and Disko Fjord $R^2 = 0.78$). There was no clear trend in NO_x^-, although in both cases NO_x^- concentrations were low, with all but one datapoint from the two catchments <0.6 μM. The observed trends and concentrations are similar to the stratified low-nitrate summertime conditions reported elsewhere around Greenland under similar conditions, for example, Young Sound (Holding et al., 2019; Sejr et al., 2022) and Ameralik (Krause et al., 2021; Stuart-Lee et al., 2021).

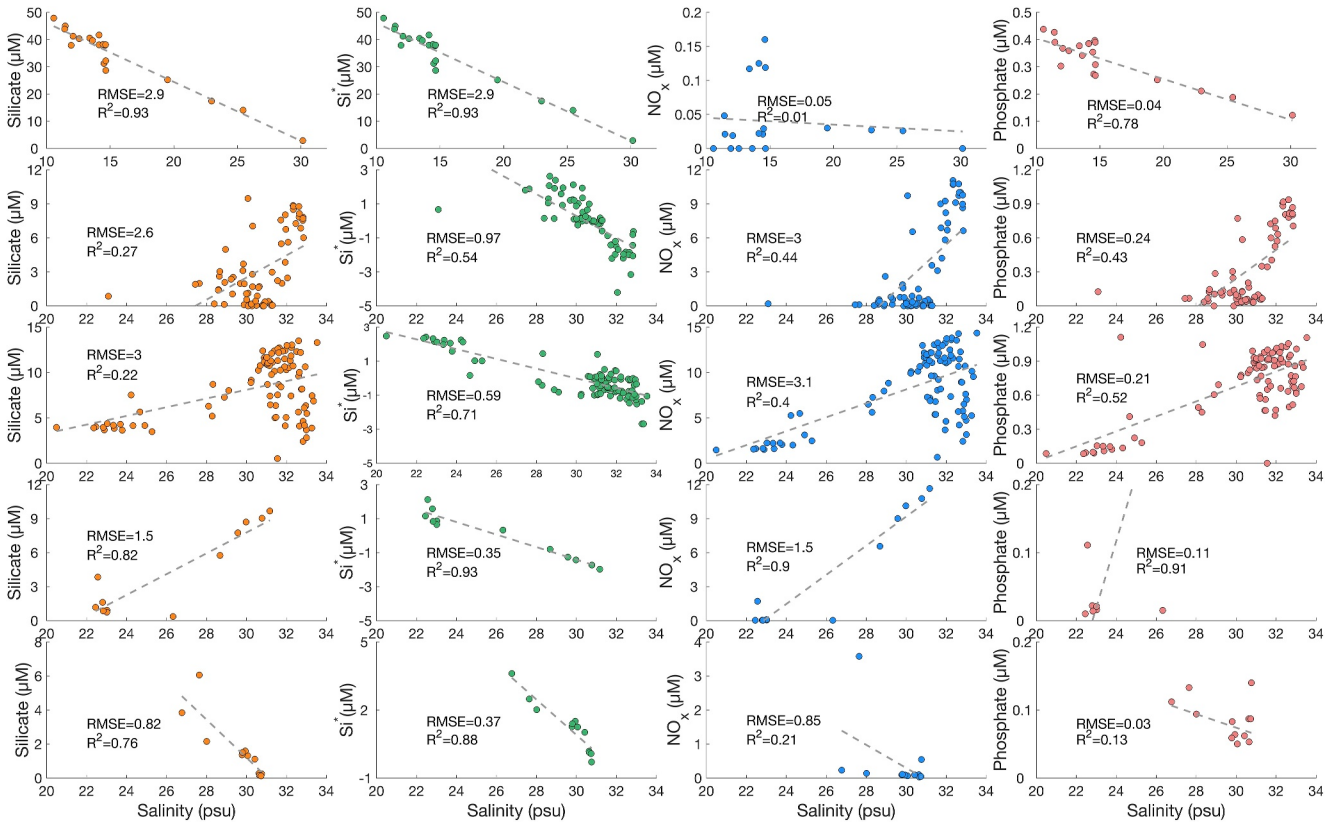

Figure 4. Nutrient-salinity relationships for five low salinity plumes in Disko Bay. Regions as per Figure 2: (1) Disko Fjord, (2) Atâ Sund and the approach to Eqip Sermia, (3) Ilulissat Icefjord, (4) Saqqarleq Fjord and the approach to Saqqarliup Sermia, and (5) Kangersuneq. Si* was calculated as dSi-NO_x^-. Linear regressions are shown. Data for areas (1) and (5) refer to underway data. Data for areas (2) and (3) include depth profiles to 100 m. Data for area (4) include depth profiles to 40 m.

Other regions had more complex trends due to the presence of both runoff and entrained sub-surface nutrient plumes. In these estuaries, the estuarine mixing diagrams (Figure 4) include profiles within the respective fjord systems (as per Figure 2) in order to capture the effects of the subsurface glacially modified waters identified in prior work (Cape et al., 2018; Gladish et al., 2015; Oliver et al., 2023). Trends in dSi were less linear and often showed increasing dSi concentrations with salinity for salinities <30 psu. Nutrient distributions with increasing concentrations at higher salinity were not unique to dSi and similar trends were observed in NO_x^- and PO_4^{3-} data (Figure 4). This indicates that mixing processes were a key driver of these trends because mixing of water masses would affect all macronutrients simultaneously (e.g., Bhatia et al., 2021; Kanna et al., 2018; Meire et al., 2017). Conversely, direct macronutrient enrichment from glacier-associated processes is primarily limited to dSi (Cape et al., 2018; Halbach et al., 2019; Meire et al., 2016).

Dense ice mélange in the Icefjord likely suppressed utilization of macronutrients by phytoplankton due to light limitation during summer and this is evidenced by gradients in nutrients observed close to the ice edge. Surface concentrations of up to 12 μM NO_x^- were found within the immediate vicinity of the ice mélange edge on the northern side of the Icefjord (Figure 2, box 1) close to Ilulissat (<50 m away from un-navigable dense ice cover, salinity 30.59–31.64 psu). These are extremely high concentrations for surface summertime water in the Arctic or Atlantic (Boyer et al., 2018). Concentrations on the southern shore in the opening of Saqqarleq Fjord (Figure 2, box 1) were still elevated above those observed in Disko Bay, but lower than those at the northern edge of the fjord mouth, ranging from 1.6 to 2.2 μM (salinity 20.49–23.34 psu). In both cases, macronutrient concentrations declined to lower and more typical NO_x^- concentrations within ~500 m from the ice edge.

Relatively high concentrations of glacier-derived aSi are expected in near-shore turbid plumes; therefore, these areas were targeted for filtration of water for aSi analysis of suspended particles. In the two main runoff sources to Saqqarleq Fjord, aSi concentrations were 110 and 123 μM, which are comparable to values reported further south in western Greenland (Hatton et al., 2023; Hawkings et al., 2017). In the turbid plumes within Disko Fjord (box 1,

Figure 2), in Kangersuneq (box 5, Figure 2), and at the entrance to Ilulissat Icefjord (box 3, Figure 2), where no particle plume was visible at the surface, aSi concentrations were much lower, ranging 0.8–6.3 μM (Figure S4 in Supporting Information S1). Assuming simple dilution of a zero salinity aSi runoff source, measured aSi concentrations in the glacier estuaries herein would correspond to ∼1%–59% of that expected from dilution. However, at higher salinity, measured aSi likely includes some biogenic aSi formed from dSi and does not simply reflect glacier-derived aSi being progressively diluted. This is evident when comparing the highest and lowest salinity stations where filters for aSi analysis were retained. For the two highest salinity stations (salinity 31.1–31.2 psu), low (below detection, <0.03 μM) dSi concentrations occurred alongside 5× higher chlorophyll *a* concentrations than other sites and 1.2–1.8 μM aSi (Figure S4 in Supporting Information S1). This is equivalent to 42%–59% of the glacier-derived aSi if we, probably erroneously, assume no biogenic aSi was present. Conversely, for the five low salinity ($S < 20$ psu) stations, aSi was 1.2%–9.1% of that expected from dilution and dSi remained >30 μM.

Bulk glacier flour samples collected from Saqqarleq Fjord, Kangerlussuaq, and a sediment coated iceberg in the Ilulissat Icefjord all had relatively low aSi content of 0.44–6.0 μmol g^{-1} (Table S1 in Supporting Information S1). The aSi content of suspended particles in runoff was higher: approximately 197 μmol g^{-1} (Kangerlussuaq), 75.5 μmol g^{-1} (Saqqarleq Fjord west), and 334 μmol g^{-1} (Saqqarleq Fjord east). Fine suspended particles in runoff thus had an aSi content a factor of 30–400 higher than coarse aged glacier flours collected from river banks and from a disintegrating iceberg at the same sites (0.44–6.0 μmol g^{-1}). Suspended particles from runoff streams were analyzed wet after collection on filters so the concentrations presented are precise based on the filtered volume of water but less precise when normalized to dry sediment load. Dry sediment load was determined on separate filter fragments as approximately 0.96 g L^{-1} (Kangerlussuaq runoff), 1.46 g L^{-1} (Saqqarleq Fjord west runoff) and 0.37 g L^{-1} (Saqqarleq Fjord east runoff).

4.3. Controlled Experiments to Assess dSi Mixing Dynamics

Observed salinity trends were typical of Greenland's coastal regions in summer, with salinities of ∼20 psu found within ∼1 km of glacier fronts in a shallow near-surface layer (Kanna et al., 2018; Mortensen et al., 2020; Murray et al., 2015). As is the case elsewhere, the transition from zero to intermediate salinities must be rapid, taking place on short spatial scales and accordingly short timescales of minutes to hours. To investigate mixing during this timeframe, unfiltered runoff was mixed with filtered saline water and incubated in the dark for 48 hr. The dSi concentration of runoff measured after 48 hr was then compared to the supposed concentration if conservative mixing had occurred. Three runoff sources were used: one from the east shore of Saqqarliup Sermia, one from the west shore of Saqqarliup Sermia, and one from Kangerlussuaq. These were mixed with the same filtered saline endmember. Coincidently, the three runoff samples were found to approximately cover the observed range of dSi in runoff with a low, average, and medium-high dSi concentration compared to typical Greenland runoff. Concentrations of dSi in the runoff when collected (12.8, 24.9, and 29.3 μM), and at the end of the experiment 1–2 weeks later (13.7, 23.3, and 31.7 μM; Figure 5) were similar. The concentrations of aSi in the initial runoff when collected were high (123, 110, and 189 μM). The initial seawater dSi concentration was 11.3 μM, which is similar to the saline endmember in all of the fjords studied herein. In all cases, quite conservative behavior of dSi was observed over 48 hr (Figure 5). These experiments were designed primarily to test the rapid release of dSi from lithogenic aSi phases in the absence of significant diatom growth. The setup will also have excluded some bacteria which in other ocean environments play a key role in the remineralization of biogenic silica- which is also aSi (Bidle & Azam, 1999). In glacier plumes, however, the main dissolution mechanism for aSi is thought to be inorganic and biogenic silica is likely a small fraction of aSi compared to the high micromolar concentrations of lithogenic aSi present. Similarly, zooplankton or other filter feeders may affect aSi dynamics in situ but are probably not major influences within turbid glacier plumes because high particle loads are associated with unproductive ecosystems (Holding et al., 2019; Stuart-Lee et al., 2023) and can be fatal to grazing filter feeders (e.g., Fuentes et al., 2016).

4.4. Controlled Experiments to Assess dSi Release Rates From Suspended Particles

Experiments at sea (Figure 5) were designed to test the effects of mixing between saline and freshwater on dSi release rates over time periods relevant to the residence time of glacier rock flour in the marine water column. Upon return to the laboratory, incubations were conducted to investigate the rate of dSi release from glacier rock flour under controlled conditions over longer time periods (up to 1 month). As limited quantities of suspended

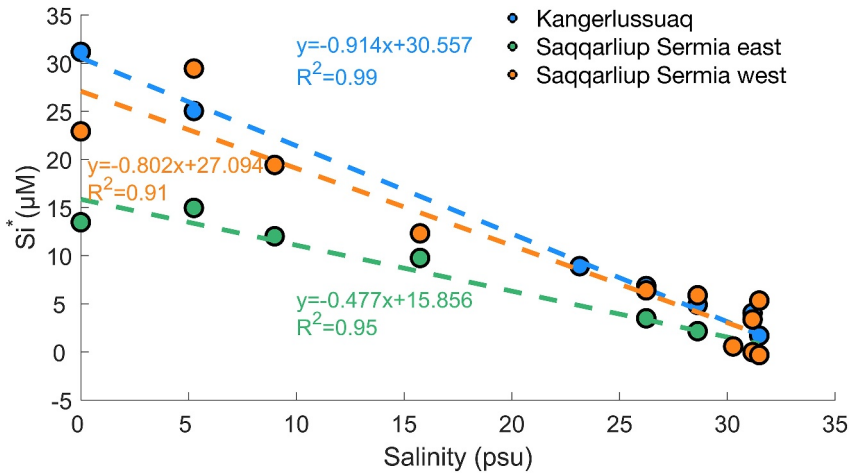

Figure 5. Mixing experiments incubating unfiltered glacier runoff with filtered coastal seawater. Three different runoff sources (blue, Kangerlussuaq; orange, Saqqarliup Sermia west; green, Saqqarliup Sermia east) were each mixed in 8 different ratios with seawater ranging from 100% runoff to 100% seawater. All aliquots were incubated at 6°C for 48 hr. Final concentrations (after 48 hr) are shown with a linear regression.

particles could be collected, four suspended rock samples were incubated at ∼50 mg L^{-1} whereas bulk glacier rock flour, which is more easily collected, was incubated with varying conditions of 10, 50 and 100 mg L^{-1} (all at 15°C). A steady release of dSi was evident from fine suspended samples with time. The total dSi released after >3 weeks was equivalent to 23%–42% of the aSi measured in fine suspended samples (Figure 6). For coarser samples of bulk glacier rock flour, changes in dSi concentration were minor (within uncertainty of the baseline in most cases) with less clear evidence for a sustained release of dSi with time (Figure S6 in Supporting Information S1). For this experiment (Figure 5 and Figure S6 in Supporting Information S1) the initial dSi concentration was intentionally low, 1.01 ± 0.06 μM, to minimize the possibility of any saturation effects. Saturation effects associated with high dSi concentrations may therefore be more important in situ in inner-fjord environments where aSi is released alongside moderately high concentrations of dSi (Figure 4, Figure S4 in Supporting Information S1).

4.5. Silica in Outflow From the Ilullisat Icefjord

Profiles at the ice mélange edge evidenced high macronutrient concentrations at depths from the surface to between 60 and 100 m depth where concentrations returned to background levels (Figure S5 in Supporting Information S1). This is a classic signature of entrained nutrient plumes (Hopwood et al., 2018; Kanna et al., 2018; Meire et al., 2017) and is similar to prior observations at the same site (Cape et al., 2018). Buoyant plumes are well characterized as drivers of upwelling in glacier fjords around Greenland (Beaird et al., 2018; Slater et al., 2022; Straneo & Cenedese, 2015), but it should be noted that they often achieve neutral buoyancy at depth (Carroll et al., 2016). The average plume neutral buoyancy depth around Greenland is estimated to be ∼100 m (Slater et al., 2022) and there may also be strong seasonal or inter-annual variation associated with changing stratification and subglacial discharge (Carroll et al., 2016). For example, prior work in Saqqarleq Fjord found a surface reaching plume in July 2013, but estimated that the plume was confined to sub-surface depths in July 2012 at the same site (De Andrés et al., 2020). In the specific case of Ilulissat Icefjord, the bathymetry of the sill, which is ∼245 m in the north and shoals to <150 m in the south (Schumann et al., 2012), and rotational effects in the relatively wide fjord (Inall & Gillibrand, 2010) may impact where positive nutrient anomalies associated with plume outflow are evident. The large surface area of calved ice within the fjord probably also exerts some profound influences on circulation due to boundary effects and form drag (Davison et al., 2020). Nevertheless, Icefjord inflow and outflow dynamics do appear to be relatively predictable on interannual timescales as the density of inflow was confined to a relatively narrow range $27.20 \leq \sigma_\theta \leq 27.31$ kg m^{-3} over three decades to 2014 (Gladish et al., 2015).

It should also be noted that nutrient concentration changes from buoyant plume entrainment, referred to as anomalies, are generally shifted to shallower depths than the peak of the glacially modified plume (Oliver

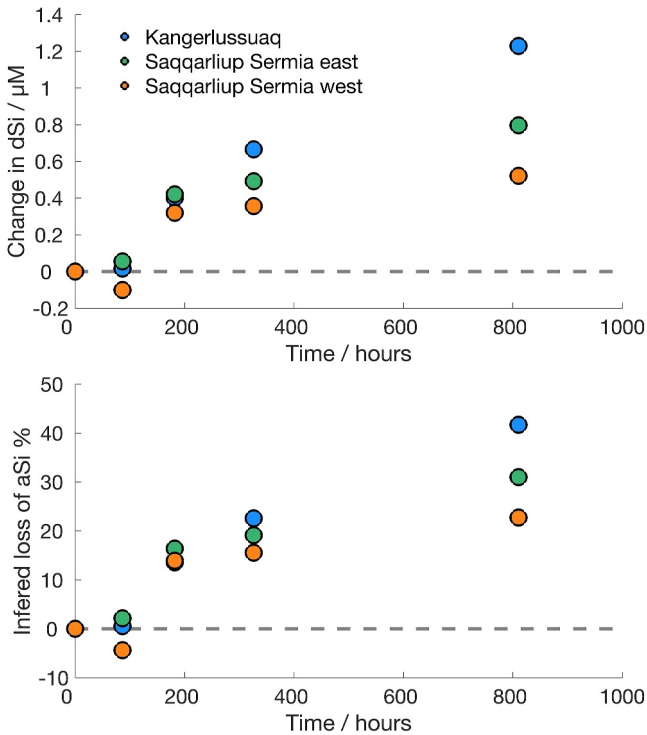

Figure 6. Release of dSi during incubation experiments with fine suspended particles from glacier runoff subjected to continuous shaking in the dark (50 mg L^{-1}, 15°C, 40 rpm). *Top*: Change in dSi concentrations during a series of experiments using fine suspended sediment from three proglacial rivers (aSi 4.5–20 mg g^{-1}) added to low dSi seawater (initial concentration 1.01 µM). *Bottom*: dSi released as a fraction of aSi present for the same experiment, assuming aSi dissolution was the only driver of changing dSi.

et al., 2023). This is because they are most evident when the background nutrient concentrations are low, that is, above the nutricline. One way of visualizing these trends is as a nutrient anomaly relative to an unperturbed water column (Figure S5 in Supporting Information S1). We defined the nutrient anomaly for the Icefjord outflow as the difference in nutrient concentrations contrasting depth profiles over the sill at the ice mélange edge, with those in Disko Bay without local glacier influence (Flux Gate B in Figure 1, see also Methods 1 in Supporting Information S1). A positive NO_x^-, dSi and PO_4^{3-} anomaly was present at all stations over the Icefjord sill (Figure S5 in Supporting Information S1). The highest NO_x^- and dSi anomalies (up to 10.6 ± 1.9 µM dSi and 11.5 ± 2.2 µM NO_x^-) were observed in near-surface waters. These anomalies cannot be directly converted into fluxes without modeling fjord outflow, but they can be scaled to the corresponding salinity anomalies in the same depth range. Compared to a reference salinity of 33 psu, the additional freshwater anomaly for the same depths was 0.60%–2.0%. The depth integrated NO_x^-, dSi and PO_4^{3-} anomalies therefore correspond to 794 ± 253, 777 ± 238, and 53 ± 16 µmol, respectively, per liter of freshwater. These values are far too high to be explained by the low concentrations in runoff (<1.6 µM NO_x^-, <33 µM dSi, <0.2 µM PO_4^{3-}) or ice melt (<2.0 µM NO_x^-, <3.5 µM dSi, <0.3 µM PO_4^{3-}).

The ratio of dSi: NO_x^- in Disko Bay for all available observations is 0.91 ± 0.27 for the density range observed to flow into the Icefjord (range 27.20 ≤ σ_θ ≤ 27.31 kg m^{-3}, Gladish et al., 2015). This ratio is within the uncertainty of the ratio in Icefjord outflow in August 2022, 0.98 ± 0.43. The net change in the dSi:NO_x^- ratio during the ~1 month residence time of saline water in the Icefjord is therefore small relative to the uncertainty, +0.07 ± 0.51. The uncertainty on this deduction could be reduced with sustained observations in the fjord mouth, but in any case, it is clear that the effects of freshwater dSi inputs on the outflowing dSi:NO_x^- ratio are minor. Deducting the change in nutrient concentrations expected from addition of freshwater (~1.2% by volume) from the observed nutrient anomaly makes only minor differences to the nutrient concentrations or ratios observed in outflow. Deducting runoff (24.9 µmol L^{-1} dSi, 0.60 µmol L^{-1} NO_x^-) as a high dSi freshwater endmember would only change the dSi:NO_x^- ratio in the outflowing plume to 0.95. Deducting iceberg meltwater as a "low" dSi freshwater endmember (0.17 µmol L^{-1} dSi, 0.83 µmol L^{-1} NO_x^-) would make no change to the outflowing dSi:NO_x^- ratio, which remains 0.98. In other words, the fraction of dSi in the outflowing positive nutrient anomaly attributable to freshwater input is only 0.2%–3.2% (Table S3 in Supporting Information S1). It should be noted that these calculations assume that all of the changes in the dSi: NO_x^- ratio within the Icefjord can be attributed to dSi sources. Any processes that removed NO_x^- without a concurrent, proportional drawdown of dSi would thereby be misinterpreted as a dSi source rather than a NO_x^- sink. Such processes could plausibly include some degree of under-ice primary production by non-siliceous microalgae, for example, or a degree of denitrification. Never-the-less, the high concentrations of all macronutrients in the fjord outflow show that any nutrient sinks within the fjord must be minor.

Whilst buoyant plume theory explains why elevated concentrations of all nutrients outflow from the Icefjord, and why the distribution of NO_x^-, dSi and PO_4^{3-} remain similar (Figure 6), this does not exclude the possibility of other nutrient sources within the fjord. We cannot deduce the entrained nutrient flux at the calving ice front for Sermeq Kujalleq (Flux Gate A, Figure 1) as our closest observations are >50 km downstream (Figure 1). The ice covered nature of the Icefjord does however produce a unique opportunity to define the outflowing nutrient fluxes at the fjord mouth. In fjords without dense ice mélange, summertime phytoplankton blooms associated with entrained nutrient plumes rapidly consume any entrained nutrient supply to the surface layer (Meire et al., 2017) such that by the fjord mouth nutrient concentrations can be depleted (Juul-Pedersen et al., 2015; Kanna et al., 2018). However, the dense ice mélange within the Icefjord over summer impedes bloom development as evidenced by high nutrient concentrations close to the surface in the outflowing glacially modified layer. The similar dSi: NO_x^- ratios of observed outflow (0.98 ± 0.43) and inflow (0.91 ± 0.27) to the Icefjord imply that the

main source of nutrient enrichment in the outflowing anomaly is the recirculation of inflowing saline waters (Methods 2 in Supporting Information S1). The recirculation of saline inflow accounts for 93 ± 51% of the dSi anomaly outflow into Disko Bay.

In future work, inert tracers of recent lithogenic particle dissolution, perhaps aluminum or titanium, may also be useful for assessing exactly where, and to what extent, water masses might have been affected by aSi dissolution or benthic effluxes in order to decouple these from recirculating dSi that originated with saline inflow. Patterns of sedimentation and turbidity in glacier fjords suggest that aSi inputs are largely confined to inner-fjord environments, so we hypothesize that most aSi dissolution (whether pelagic or benthic) takes place within glacier fjords. Whilst aSi measurements herein were only in surface waters and not adequate to test this hypothesis in outflow from the Icefjord, more extensive in-fjord aSi measurements in Nuup Kangerlua appear to support this hypothesis, with high concentrations of aSi declining to concentrations of <1 μM (which, as noted, includes biogenic silica) by the fjord mouth (Hatton et al., 2023). Later work in the same region somewhat muddies this interpretation, however, suggesting that higher aSi concentrations, both in absolute terms (1–4 μM) and normalized to meteoric water, can be found on the shelf immediately outside Nuup Kangerlua (Ng et al., 2024), perhaps implying additional sources of aSi on the shelf.

4.6. Evaluating (Non)-Conservative dSi Dynamics

A key region for studying whether or not a major non-conservative dSi source is evident from glacier activity is the near-shore zone, which was specifically targeted in five distinct estuaries that exhibited contrasting turbidity, chlorophyll and runoff dynamics (Figures 2 and 4). Whilst the underway turbidity and chlorophyll measurements are only relative, and spatial trends in turbidity may be skewed due to the slow flushing of particles through the sensor unit box, they highlight the contrasting nature of these zones. Chlorophyll was moderately low close to the ice mélange edge in the Ilulissat Icefjord, likely reflecting light limitation in the fjord itself and thus a delay between the near-surface outflow of high nutrient concentrations and the accumulation of phytoplankton stock. Furthermore, turbidity was also low, likely reflecting the sinking of particles and deposition of sediment from runoff and ice melt under the ice cover before outflowing waters enter Disko Bay at the western edge of the ice mélange. Filtration of water (20 L) from a station next to the ice edge did not yield any measurable particle load (limit of detection ∼10 mg), implying a suspended sediment load of <0.5 mg L^{-1}, but numerous live copepods were found. The same location evidenced a low aSi load in the surface waters (0.76 μM). Satellite chlorophyll data evidenced a plume of high primary production close to the Icefjord entrance, mainly along the northeast coastline of the Bay (Figure 2), which is a commonly observed seasonal feature (Oliver et al., 2023). This may reflect the pathway of outflow from the Icefjord. Satellite-derived estimates of chlorophyll within Disko Bay suggest that 2022 dynamics were similar to adjacent years (2018–2023) and that most interannual variability is associated with the more productive spring bloom period. Productivity from June-September was lower with relatively low interannual variability (Figure S7 in Supporting Information S1).

Close to Eqip Sermia, there was partial ice cover from small ice fragments (typically < 1 m length above the water line) in the inner fjord. Chlorophyll *a* was generally high, especially in the mid-fjord at ∼20 km distance from the glacier, and turbidity was high in parts of the inner-fjord. This follows the classic trends expected during summer in a marine-terminating glacier fjord with nutrient entrainment and estuarine circulation; the inner fjord evidences low chlorophyll and high turbidity due to local glacier activity, by the mid-fjord environment a bloom has developed and lithogenic particles have sedimented, and then toward the outer fjord nutrients are depleted within the photic zone and both chlorophyll and turbidity decline to lower levels (Meire et al., 2017; Oliver et al., 2020). In Kangersuneq, turbidity was high in the inner fjord, and chlorophyll never reached high values consistent with the expected effect of runoff driving strong stratification and low summertime productivity (Holding et al., 2019; Lund-Hansen et al., 2010; Meire et al., 2017). Turbidity then declined down-fjord due to particles sinking and sedimentation. In Disko Fjord, two distinct plumes of high turbidity were intercepted in the inner fjord, with turbidity declining downstream and chlorophyll remaining relatively low, again likely reflecting low productivity associated with runoff driving strong stratification in nitrate-limited summertime conditions (Randelhoff et al., 2020). Discussion of chlorophyll trends herein relies on underway and satellite data, which can underestimate chlorophyll in subsurface plumes. Subsurface chlorophyll peaks have been found in parts of the Arctic (Ardyna et al., 2017; Martín et al., 2010) but are not expected in inner-fjord areas with high turbidity due to shallow photic zones (Murray et al., 2015).

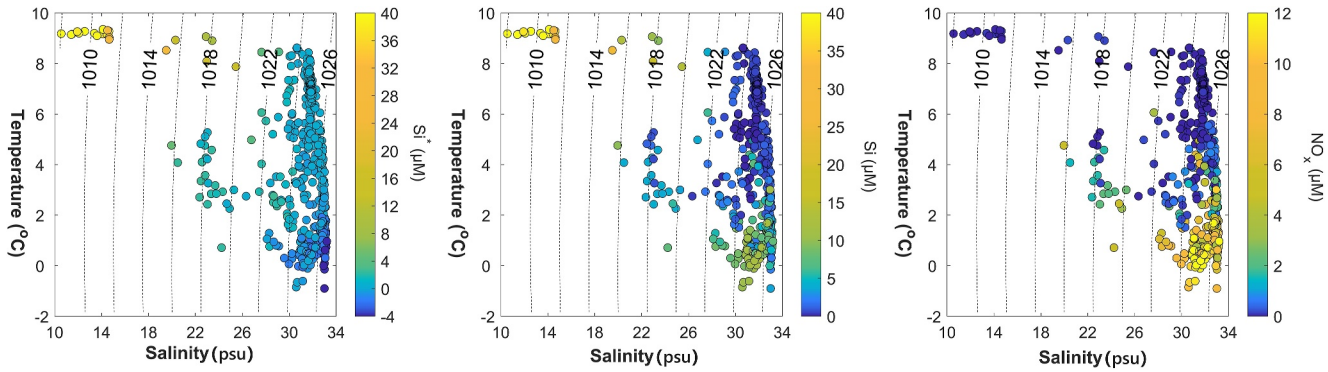

Figure 7. Density distribution of Si*, dSi and NO_x^- concentrations. Si* was calculated as dSi-NO_x^- for all data in Disko Bay. Si* approximately corrects for the dSi supplied by macronutrient rich saline waters and is therefore an approximation of dSi added by processes associated with dSi-rich, nitrate-, and phosphate-deficient concentrations.

It is not possible to assess whether or not dSi dynamics are conservative from the dSi salinity relationship alone if there is a confounding influence of subglacial discharge plumes (as per at the entrance of the Ilulissat Icefjord). Interpretation of dSi trends in a two endmember system with freshwater runoff and deep saline inflow would be relatively straightforward if we could constrain the two endmembers and they were approximately constant over the timescale of mixing. Unfortunately, most fjord systems herein and elsewhere around Greenland are not two endmember systems. Melting icebergs and multiple freshwater outflows drive spatial and temporal variation in the freshwater endmember(s). The saline inflow into fjords may resemble unmodified Atlantic Water in deep fjords without sills (Cape et al., 2018; Oliver et al., 2020). However, for fjords with multiple sills, multiple basins, uncharacterized seasonal renewal patterns, and the possibility of water mass modifications over the shelf, it is more challenging to precisely define the saline endmember (Boone et al., 2018; Mortensen et al., 2018). However, whilst the precise endmember dSi concentrations may be uncharacterized, the dSi:NO_3^- ratio of the key source terms and processes are much better known. Diatom drawdown of dSi:NO_3^- is well defined at 1:1 (Brzezinski, 1985), dSi:NO_3^- in water masses around the Greenland shelf is density-dependent and relatively invariable (Boyer et al., 2018) compared to the strong changes at low salinities, and freshwater source terms have an extremely high dSi:NO_3^- ratio compared to any saline water mass (Meire et al., 2016). Accordingly, either dSi:NO_3^- or dSi-NO_3^- could be used to trace any local dSi anomalies associated with glaciers (Torres et al., 2014). Si* is more easily applicable to low NO_3^- environments as it is less sensitive to issues caused by nutrient data being close to, or below, the detection limit.

The inflow/outflow dynamics of Greenland's fjords mean that the concentrations of dSi and NO_x^- are approximately proportional in deep inflowing water (e.g., for the Icefjord 0.91 ± 0.27, Methods S1 in Supporting Information S1), whereas the concentration of dSi in runoff is normally vastly in excess of NO_x^- and PO_4^{3-} (e.g., dSi:NO_3^- ranges from 19 to 42 for runoff in Disko Bay herein, and from 3 to 190 for the compilation by Meire et al., 2016). Over small spatial scales, Si* (or dSi:NO_3^-) can therefore be used to assess whether or not there is an approximately conservative mixing line between two endmembers in a system where runoff and nutrient entrainment both strongly influence dSi dynamics. This will remain the case as long as it can be approximated that all freshwater has approximately the same dSi concentration. In a system where there are both high and low dSi:NO_3 freshwater sources, conservative mixing would instead be bounded by a triangle defined by: saline, "high" dSi freshwater, and "low" dSi freshwater endmembers.

Analysis of Si* versus salinity reveals very different trends compared to the dSi plots in some estuaries/fjords (Figures 4 and 7) and confirms that mixing effects were indeed a strong influence on the observed dSi trends in high salinity waters (Figures 4 and 7). All estuarine regions studied, except Eqip Sermia, had an approximately linear Si* relationship with salinity (Icefjord $R^2 = 0.71$, Disko Fjord $R^2 = 0.93$, Kangersuneq $R^2 = 0.88$, Saqqarleq Fjord $R^2 = 0.93$, and Eqip Sermia $R^2 = 0.54$). The main caveat with this calculation, as noted, is that it assumes a single freshwater endmember and a single saline endmember. In reality, most of these fjords contained multiple runoff sources in addition to melting icebergs, which had low dSi concentrations (measured dSi 0.11 ± 0.41 μM) compared to runoff (measured dSi 24.9–32.0 μM). Kangersuneq and Disko Fjord best

approximated simple systems, each with two main point sources of runoff, low chlorophyll and no direct calving of icebergs into the fjord. This likely explains why these systems exhibited the strongest linearity in the Si*-salinity relationship (Figure 4).

The Ilulissat Icefjord entrance likely integrates freshwater outflow from several upstream systems superimposed on ice melt, but these sources may be relatively well mixed in the surface layer by the time these waters reach the ice mélange edge, due to the long along-fjord distance between the marine-terminating glacier fronts and fjord mouth (>50 km). This could result in a Si* relationship that is still approximately linear despite the presence of two distinct freshwater endmembers with different dSi concentrations (runoff and iceberg melt). Nutrient anomaly calculations also show that inflowing saline water is the dominant nutrient source to the plume; hence, Si* changes are limited compared to other fjords where runoff is relatively more important as a dSi source. Eqip Sermia similarly neighbours several different marine-terminating glaciers and runoff streams entering the same fjord in close proximity to the sampled cruise track. The lowest salinity datapoints within the fjord were within the outflow plumes of a proglacial river on the opposite shoreline to Eqip Sermia rather than close to the main marine-terminating glacier. When these points are removed, the linear trend improves (e.g., from $R^2 = 0.54$ to $R^2 = 0.66$ if the 3 low salinity points associated with secondary freshwater outflows are not considered). Dynamics within the fjord may therefore approximate conservative mixing, but additional tracers would be required to confirm this in order to quantify the fractions of different freshwater endmembers.

Turbidity data herein suggests a decline to background values at 1 m depth within <20 km of glacier fronts, which may be an over-estimate due to the slower flushing of particles than water from the underway sensor box units. Similarly, aSi concentrations declined much faster than dSi concentrations with increasing salinity, evidencing the rapid sinking of particles in the marine environment. This is consistent with sediment records which suggest intense deposition of glacier rock flour within a few kilometers of the terminus in most cases (Dowdeswell et al., 1998; Smith & Andrews, 2000; Syvitski et al., 1996). To our knowledge, the only particle residence time calculations available, from Ameralik in southwest Greenland, suggest a residence time of ∼1 day for runoff derived particles using the estimated input of 3 g L^{-1} glacial rock flour and a 20 m deep, 400 km^2 suspended particle plume of 6–9 mg L^{-1}` (Stuart-Lee et al., 2023; Zhu et al., 2024). This is generally consistent with the above observations considering the plausible rate of down-fjord flow in the surface layer. A mixing experiment of approximately this duration is therefore a good indicator of the magnitude of dSi release that should be expected from glacier rock flour over the timescale during which particles remain in suspension (Figure 5). Using three different runoff sources, the change in dSi concentration over this time period was limited. This is consistent with the generally linear Si* trends observed herein for in situ data (Figure 4) and suggests that significant aSi dissolution could only occur in the benthos where particles are resident for much longer than in the water column. Slow rates of aSi dissolution to release dSi were further evident in >3 week incubation experiments under controlled laboratory conditions (Figure 6). In the laboratory, the particles were constantly mixed (40 rpm), whereas in situ flocculation dynamic likely results in particle aggregation with fewer particle collisions. Therefore, dissolution rates under laboratory conditions may be higher than in situ. In any case, it seems likely that conversion of aSi to dSi within the water column over the ∼1 day residence time of suspended particles produces a release of dSi of the order of 1% of aSi.

Benthic dSi fluxes likely change along fjord gradients (Ng et al., 2020) due to the typical change in sediment composition induced by prolific glacial flour deposition at fjord heads and lateral changes in pelagic primary production (Jørgensen et al., 2021; Zajączkowski & Włodarska-Kowalczuk, 2007). These fluxes were not quantified herein and no regional measurements are available for Disko Bay. Given the much longer residence time of glacier-derived aSi in benthic environments, the benthic realm may be more important than the pelagic realm for aSi dissolution. Yet, this will clearly be moderated by very different factors due to the different environmental contexts. Nevertheless, the circulation of deep glacier fjords means any accumulated benthic dSi release during the ∼1 month timeframe of saline inflow should be evident in the outflowing surface layer alongside any other dSi inputs (Figure 1).

The intercepts derived from Si* plots in low-productivity estuaries (e.g., Disko Fjord 68 μM, Kangersuneq 24 μM, and Ilulissat Icefjord 9.4 μM) should approximate the combined dSi input from direct freshwater dSi additions, aSi dissolution occurring in freshwater, and aSi derived dSi additions occurring while particles are in suspension in the surface layer. Moderately high extrapolated freshwater dSi endmembers were determined herein, especially in Disko Fjord, but these are consistent with the reported distribution of dSi around Greenland

in runoff (Meire et al., 2016; Yde et al., 2005), and are much smaller than what would be expected if aSi were rapidly converted to dSi at low salinities. Using a pan-Greenland estimate of aSi concentrations in runoff, the mean extrapolated freshwater endmember for a scenario with efficient conversion of aSi to dSi in low-salinity waters would be 400 μM (9.6 μM dSi + 392 μM aSi, Hawkings et al., 2017). Conversely, a 1% dissolution of aSi prior to burial would increase the apparent freshwater endmember about 4 μM, or roughly 15% for estuaries with typical runoff dSi concentrations in west Greenland. The latter scenario is consistent with the observed fjord-scale aSi and dSi distributions. This is in addition to any aSi dissolution occurring within deep saline layers. Any aSi dissolution occurring in deep saline layers (whether pelagic or benthic) would be difficult to constrain from estuarine mixing plots without a specific tracer of aSi dissolution, but should be included within entrained nutrient calculations which represent the transfer of dSi from the deep to surface layers (i.e. Flux Gate A, Fig, 1). In Nuup Kangerlua, for example, entrainment supplies 12% of dSi to the surface layer in summer (Meire et al., 2016). A large fraction of this likely originates from saline inflow to the fjord, as per the case of the Icefjord, but aSi dissolution may also contribute.

4.7. Revisiting Greenland Ice Sheet-Ocean dSi Flux Calculations

Although subject to moderate uncertainties, the unique case study of the Ilullisat Icefjord corroborates saline recirculation as the major driver of positive nutrient anomalies outflowing into Disko Bay and suggests that supplementary inputs of dSi from glaciers are small by comparison. It is therefore prudent to re-visit the assumptions that underpin a high contribution of Greenland derived aSi to annual dSi budgets. A non-linear dSi-salinity trend in Kangerlussuaq was in prior work assumed to represent non-conservative processes, which must have been rapid enough to lead to dSi increasing over the salinity gradient (Hawkings et al., 2017). However, as shown herein, non-linearity is relatively common in fjord dSi-salinity distributions due to multiple freshwater endmembers and mixing processes (Figure 4). Non-linearity alone is not therefore sufficient evidence of non-conservative behavior unless also evident in Si* plots. Additionally, suspended particles from Kangerlussuaq, and two other outflows, did not evidence a dSi release large enough or fast enough to explain a large "missing" source of dSi in estuaries. Amorphous Si dissolution rates herein are consistent with those measured in prior work (Hawkings et al., 2017), suggesting that particles do not remain in suspension long enough to facilitate dSi release as a major budget term in the marine environment, especially not in the surface outflowing layer of glacier fjords. Inefficient aSi dissolution in such layers is consistent with the similar zero-salinity intercepts from Si* salinity plots and measured freshwater dSi concentrations (Figure 4) (Azetsu-Scott & Syvitski, 1999; Cape et al., 2018; Holding et al., 2019; Kanna et al., 2018; Lund-Hansen et al., 2018; Meire et al., 2017).

Later work in Nuup Kangerlua, perhaps the best studied site in Greenland for coastal nutrient dynamics (Juul-Pedersen et al., 2015; Meire et al., 2016, 2017), suggested that a large gross release of dSi from suspended aSi occurs within the fjord (Hatton et al., 2023) but is not evident in dSi trends because there is a roughly equivalent drawdown of dSi by diatoms. The diatom drawdown of dSi could thereby roughly counter-balance the release of dSi from aSi in the surface layer- if these processes occurred with similar rates and spatial scales- and thus produce a pseudo-conservative dSi-salinity plot. Diatoms are a major component of spring and summer time blooms in Greenland's coastal waters (Krawczyk, Arendt et al., 2015; Krawczyk, Witkowski et al., 2015; Krawczyk et al., 2018; Luostarinen et al., 2020) and their high contribution to primary production in Nuup Kangerlua has been constrained (Krawczyk, Arendt et al., 2015; Krawczyk, Witkowski et al., 2015; Krawczyk et al., 2018; Meire et al., 2017). A prior dSi budget for Nuup Kangerlua estimated a combined iceberg, runoff and subglacial discharge plume (inclusive of entrainment) input to the mixed layer of 1.0 ± 0.2 Gmol dSi $year^{-1}$ (Meire et al., 2016). This can be slightly refined with more recent data (Methods 2 in Supporting Information S1), although the only large change is to reduce the estimate of iceberg dSi delivery (Krause et al., 2024).

Compared to the estimated diatom productivity in Nuup Kangerlua (Methods 2 in Supporting Information S1), dSi demand is 41%–144% of the dSi inputs calculated for the surface layer. This suggests that dSi supply and demand within the fjord are approximately balanced. Outflow from Nuup Kangerlua is well constrained year-round from a monitoring station in the fjord mouth, which shows a dSi concentration of 2.17 ± 1.03 μM (depths <40 m, May–August) (Juul-Pedersen et al., 2015; The Greenland Ecosystem Monitoring (GEM) Database). The existing dSi budget proposed by Meire et al. (2016) is therefore consistent with both measured diatom productivity within the fjord and the dSi time-series at the fjord mouth, which suggests no large net dSi outflow (dSi concentrations are higher at depth in inflowing saline waters). This budget also already includes a term to describe the vertical transfer of dSi from the deep, saline layer to the surface layer, corresponding to Flux Gate A

(Figure 1) which should include any sources of dSi to the deep layer (including aSi dissolution). Similarly, aSi dissolution occurring in freshwater or over short (<1 day) time periods after freshwater is released into the fjord should already be reflected in the budget which is constructed from observed dSi concentrations.

It is therefore difficult to explain how an additional large net aSi-derived source of dSi could be invoked within Nuup Kangerlua and maintain consistency with existing observations. If aSi concentrations supplied to Nuup Kangerlua annually approximated those used as a Greenland average (392 μM for runoff and 49 μM for icebergs, Hawkings et al., 2017), which seems reasonable -or perhaps an underestimate- based on measured aSi concentrations observed within Nuup Kangerlua (Hatton et al., 2023), and we assume this aSi is converted quantitatively to dSi (Hawkings et al., 2017), this would increase total dSi inputs for Nuup Kangerlua (inclusive of entrainment) by a factor of 11. Observed primary production in Nuup Kangerlua now accounts for 4%–15% of the annual dSi supply. In other words, the fjord would be a considerable source of dSi to the shelf, and diatom drawdown of dSi would only remove a fraction of the dSi supplied to the surface layer within the fjord. Both of these suggestions are not consistent with field observations and so it can be summarized that only a small fraction of aSi could possibly be made available to diatoms on annual timescales within the fjord. To explain the δ^{30}Si signature of dSi within Nuup Kangerlua, Hatton et al. (2023) deduced that about 0.04%–25% of aSi must dissolve within the fjord. Values at the lower end of this range are consistent with both the above dSi budget for Nuup Kangerlua, and the interpretation of estuarine mixing diagrams for dSi in glaciated catchments around the Arctic (Cantoni et al., 2020; Kanna et al., 2018; Meire et al., 2016). Similarly, incubation experiments suggest a net dSi release in glacier estuaries on the order of 1% of the aSi present in glacier runoff. As noted, these values are not strictly additive however. Strictly speaking, only aSi dissolution occurring in the surface layer after rapid mixing processes at the glacier fronts is not already included in the Nuup Kangerlua dSi budget as parameterized by Meire et al. (2016). With benthic dSi inputs largely confined to the deep layer, and a short residence time of particles in the surface layer, the majority of aSi dissolution occurring is likely already included within the entrained nutrient flux calculation (see Methods 2 in Supporting Information S1).

These deductions do not necessarily mean that aSi is not slowly converted to dSi with high efficiency in terrestrial freshwater environments or after deposition in fjord sediments. In the Disko Bay region, aSi values for the fine suspended particles in runoff (4.5–20 mg g^{-1}) were comparable to those previously reported in Kangerlussuaq (5.1–12.1 mg g^{-1}) and much higher than those present in coarse glacier flour (0.027–0.036 mg g^{-1}). The lower aSi concentrations in coarse glacier flour could reflect a combination of a surface area effect, and aging resulting in gradual washout of aSi. The associated dSi release in freshwater environments is accounted for in estimates of runoff dSi when runoff dSi concentrations are measured at the coastline, and likely contributes to the large increase in dSi concentrations between ice melt (0.41 ± 1.11 μM) and runoff (~22–27 μM) around Greenland. In the case of benthic release of dSi into fjord environments, the incubation experiments herein poorly represent the benthic environment where particles are less mobile, dSi concentrations higher, and other factors regulate dSi release into the water column. It can however be deduced from the fjord-scale dSi budget in Nuup Kangerlua and the Icefjord, and more generally from the status of fjords as nutrient sinks, that net benthic release of dSi must be a minor source of dSi to fjord-scale budgets.

We stress that how aSi is included within budgets of Greenland's contribution to the global silica cycle makes a considerable difference to the calculated annual contribution. Inclusion of lithogenic aSi from Greenland, assuming it will be efficiently converted to dSi in the ocean and is not already partially included in runoff dSi fluxes, produces an annual flux of 0.2 Tmol yr^{-1} (Hawkings et al., 2017). On the other hand, assuming any conversion of aSi to dSi is already accounted for in measured runoff concentrations at the coastline with no significant further release after particles outflow into the ocean produces a much lower flux of 14 ± 5 Gmol Si yr^{-1} (Meire et al., 2016). Based on a combination of in situ observations and incubation experiments, we infer that approximately 1% of aSi is converted to dSi during the short (~1 day) residence time of glacier-derived aSi in pelagic environments. Using a prior estimate of 0.19 Tmol $year^{-1}$ aSi outflow from icebergs and runoff around Greenland, this would correspond to a dSi release of approximately 1.9 Gmol dSi $year^{-1}$ (increasing the runoff dSi flux from Greenland by approximately 12%). This estimate is consistent with earlier interpretations of the limited available estuarine mixing curves for dSi in Arctic glacier estuaries, which suggest dSi additions equivalent to ~10% of that sourced from runoff (Hopwood et al., 2020). An additional benthic component of aSi release is not specifically constrained herein, but likely makes an additional minor contribution to the annual dSi budget within glacier fjords as a fraction of the entrained dSi flux (Flux Gate A, Figure 1).

5. Conclusions

Si* salinity relationships simplify the interpretation of dSi patterns in Arctic fjords with marine-terminating glaciers, where entrainment of macronutrients in discharge plumes complicates nutrient-salinity relationships. Si* relationships generally indicate conservative dSi dynamics in Disko Bay and are similar to trends observed elsewhere around Greenland (Azetsu-Scott & Syvitski, 1999; Cape et al., 2018; Kanna et al., 2018; Meire et al., 2016). Outflow from the Ilulissat Icefjord leads to large positive nutrient anomalies entering Disko Bay. A comparison of inflow and outflow dynamics to the Icefjord suggests that recirculation of inflowing saline water provides 93 ± 51% of the dSi anomaly outflowing into Disko Bay. Freshwater on the other hand provides only 0%–3%. These proportions differ from the better studied Nuup Kangerlua, where runoff is the dominant dSi source (87%) and entrainment in a glacier discharge plume is less important (12%). The stark difference is not unanticipated however. Idealized calculations for nitrate fluxes in prior work predicted the nitrate flux anomaly from Sermeq Kujalleq in the Icefjord to be 5–60 fold larger than the plume from Kangiata Nunata Sermia in Nuup Kangerlua (Oliver et al., 2023).

Dissolved Si enrichment in the outflowing low salinity layer of glacier fjords reflects the addition of dSi from glacier runoff, with a mean dSi endmember across the five estuaries studied of 26.2 μM (range 9.4–68 μM). Dissolved Si concentrations in Disko Fjord were higher than other areas, yet this is consistent with direct measurements of dSi in runoff, which suggest that dSi concentrations on Disko Island are among the highest in Greenland (Meire et al., 2016; Yde et al., 2005). A minor additional source of dSi probably arises from net release from aSi in glacier estuaries, but this is not evident as a large flux in short-term mixing experiments matching the residence time of glacier rock flour in the marine water column. More detailed incubation experiments are required to fully constrain the additional benthic component of aSi dissolution. However, it is important to note that aSi associated dSi fluxes are not strictly additive in several budget contexts as dSi fluxes are often derived from measurements which include the net effects of any dissolution processes occurring. An overestimation of the role of the Greenland Ice Sheet in marine dSi cycling likely arises because of a misinterpretation of conservative mixing in Kangerlussuaq (Hawkings et al., 2017) based on the assumption that an increase in dSi concentrations with increasing salinity represents fast conversion of aSi to dSi. Yet in multi-plume environments an increase in dSi concentrations with increasing salinity is often observed for other reasons (Figure 4). A lower Greenland Ice Sheet flux estimate of 14.2 ± 1.5 Gmol Si yr^{-1} for freshwater outflow (Meire et al., 2016) is likely more realistic considering the results of mixing experiments and the slow release rate of dSi from aSi compared to the short residence time of glacier-derived particles in the water column. Runoff dSi sources are likely supplemented with an additional dSi input of ∼1.9 Gmol $year^{-1}$ from the release of aSi in outflowing low salinity glacier plumes and an additional contribution toward the entrained dSi fluxes from aSi dissolution within deep fjord basins. An estimate for this budget term could be deduced if a tracer were available to constrain the fraction of dSi entrained in glacier discharge plumes which represents "new" dSi from aSi dissolution, rather than recirculation of dSi from saline inflow.

Data Availability Statement

Oceanographic data used herein are available at SeaDatNet via [https://evior.eurofleets.eu/cds-report/17] with a Creative Commons Attribution (CC BY) license.

Acknowledgments
The captain and crew of RV Sanna are thanked for field support. André Mutzberg (GEOMAR) is thanked for macronutrient data, and Karl Aakattak Sandgreen and Ove Villadsen (IWS Tours) for logistics support and invaluable knowledge of the Icefjord. MH received support from the DFG (HO 6321/1-1), the GLACE project organized by the Swiss Polar Institute and supported by the Swiss Polar Foundation, NSFC project 42150610482 and the European Union H2020 research and innovation programme under grant agreement n° 824077. We gratefully acknowledge ship time coordination by EUROFLEETS+ and the Greenland Institute of Natural Resources. We thank three reviewers for constructive comments on the manuscript.

References

Alfredsson, H., Clymans, W., Hugelius, G., Kuhry, P., & Conley, D. J. (2016). Estimated storage of amorphous silica in soils of the circum-Arctic tundra region. *Global Biogeochemical Cycles*, *30*(3), 479–500. https://doi.org/10.1002/2015GB005344

Andresen, C. S., Karlsson, N. B., Straneo, F., Schmidt, S., Andersen, T. J., Eidam, E. F., et al. (2024). Sediment discharge from Greenland's marine-terminating glaciers is linked with surface melt. *Nature Communications*, *15*(1), 1332. https://doi.org/10.1038/s41467-024-45694-1

Andrews, M. G., Jacobson, A. D., Osburn, M. R., & Flynn, T. M. (2018). Dissolved carbon dynamics in meltwaters from the Russell Glacier, Greenland Ice Sheet. *Journal of Geophysical Research: Biogeosciences*, *123*(9), 2922–2940. https://doi.org/10.1029/2018JG004458

Ardyna, M., Babin, M., Devred, E., Forest, A., Gosselin, M., Raimbault, P., & Tremblay, J.-É. (2017). Shelf-basin gradients shape ecological phytoplankton niches and community composition in the coastal Arctic Ocean (Beaufort Sea). *Limnology & Oceanography*, *62*(5), 2113–2132. https://doi.org/10.1002/lno.10554

Armbrust, E. V. (2009). The life of diatoms in the world's oceans. *Nature*, *459*(7244), 185–192. https://doi.org/10.1038/nature08057

Azetsu-Scott, K., & Syvitski, J. P. M. (1999). Influence of melting icebergs on distribution, characteristics and transport of marine particles in an East Greenland fjord. *Journal of Geophysical Research*, *104*(C3), 5321–5328. https://doi.org/10.1029/1998JC900083

Beaird, N. L., Straneo, F., & Jenkins, W. (2018). Export of strongly diluted Greenland meltwater from a major glacial fjord. *Geophysical Research Letters*, *43*(9), 4163–4170. https://doi.org/10.1029/2018GL077000

Bhatia, M. P., Waterman, S., Burgess, D. O., Williams, P. L., Bundy, R. M., Mellett, T., et al. (2021). Glaciers and nutrients in the Canadian Arctic archipelago marine system. *Global Biogeochemical Cycles*, *35*(8), e2021GB006976. https://doi.org/10.1029/2021GB006976

Bidle, K. D., & Azam, F. (1999). Accelerated dissolution of diatom silica by marine bacterial assemblages. *Nature*, *397*(6719), 508–512. https://doi.org/10.1038/17351

Boone, W., Rysgaard, S., Carlson, D. F., Meire, L., Kirillov, S., Mortensen, J., et al. (2018). Coastal freshening prevents fjord bottom water renewal in Northeast Greenland: A mooring study from 2003 to 2015. *Geophysical Research Letters*, *45*(6), 2726–2733. https://doi.org/10.1002/2017GL076591

Boyer, T. P., Garcia, H. E., Locarnini, R. A., Zweng, M. M., Mishonov, A. V., Reagan, J. R., et al. (2018). *World ocean atlas 2018*. NOAA National Centers for Environmental Information.

Brzezinski, M. A. (1985). The Si:C: N ratio of marine diatoms: Interspecific variability and the effect of some environmental variables. *Journal of Phycology*, *21*(3), 347–357. https://doi.org/10.1111/j.0022-3646.1985.00347.x

Cantoni, C., Hopwood, M. J., Clarke, J. S., Chiggiato, J., Achterberg, E. P., & Cozzi, S. (2020). Glacial drivers of marine biogeochemistry indicate a future shift to more corrosive conditions in an Arctic fjord. *Journal of Geophysical Research: Biogeosciences*, *125*(11), e2020JG005633. https://doi.org/10.1029/2020JG005633

Cape, M. R., Straneo, F., Beaird, N., Bundy, R. M., & Charette, M. A. (2018). Nutrient release to oceans from buoyancy-driven upwelling at Greenland tidewater glaciers. *Nature Geoscience*, *12*(1), 34–39. https://doi.org/10.1038/s41561-018-0268-4

Carroll, D., Sutherland, D. A., Hudson, B., Moon, T., Catania, G. A., Shroyer, E. L., et al. (2016). The impact of glacier geometry on meltwater plume structure and submarine melt in Greenland fjords. *Geophysical Research Letters*, *43*(18), 9739–9748. https://doi.org/10.1002/2016GL070170

Carroll, D., Sutherland, D. A., Shroyer, E. L., Nash, J. D., Catania, G. A., & Stearns, L. A. (2017). Subglacial discharge-driven renewal of tidewater glacier fjords. *Journal of Geophysical Research: Oceans*, *122*(8), 6611–6629. https://doi.org/10.1002/2017JC012962

Davison, B. J., Cowton, T. R., Cottier, F. R., & Sole, A. J. (2020). Iceberg melting substantially modifies oceanic heat flux towards a major Greenlandic tidewater glacier. *Nature Communications*, *11*(1), 5983. https://doi.org/10.1038/s41467-020-19805-7

De Andrés, E., Slater, D. A., Straneo, F., Otero, J., Das, S., & Navarro, F. (2020). Surface emergence of glacial plumes determined by fjord stratification. *The Cryosphere*, *14*(6), 1951–1969. https://doi.org/10.5194/tc-14-1951-2020

DeFoor, W., Person, M., Larsen, H. C., Lizarralde, D., Cohen, D., & Dugan, B. (2011). Ice sheet–derived submarine groundwater discharge on Greenland's continental shelf. *Water Resources Research*, *47*(7). https://doi.org/10.1029/2011WR010536

DeMaster, D. J. (1981). The supply and accumulation of silica in the marine environment. *Geochimica et Cosmochimica Acta*, *45*(10), 1715–1732. https://doi.org/10.1016/0016-7037(81)90006-5

Dowdeswell, J. A., Elverhfi, A., & Spielhagen, R. (1998). Glacimarine sedimentary processes and facies on the polar North Atlantic margins. *Quaternary Science Reviews*, *17*(1), 243–272. https://doi.org/10.1016/S0277-3791(97)00071-1

Droghei, R., Buongiorno Nardelli, B., & Santoleri, R. (2018). A new global sea surface salinity and density dataset from multivariate observations (1993–2016). *Frontiers in Marine Science*, *5*. https://doi.org/10.3389/fmars.2018.00084

Droghei, R., Nardelli, B. B., & Santoleri, R. (2016). Combining in situ and satellite observations to retrieve salinity and density at the ocean surface. *Journal of Atmospheric and Oceanic Technology*, *33*(6), 1211–1223. https://doi.org/10.1175/JTECH-D-15-0194.1

Fuentes, V., Alurralde, G., Meyer, B., Aguirre, G. E., Canepa, A., Wölfl, A.-C., et al. (2016). Glacial melting: An overlooked threat to Antarctic krill. *Scientific Reports*, *6*(1), 27234. https://doi.org/10.1038/srep27234

Gladish, C. V., Holland, D. M., Rosing-Asvid, A., Behrens, J. W., & Boje, J. (2015). Oceanic boundary conditions for Jakobshavn glacier. Part I: Variability and renewal of Ilulissat Icefjord waters, 2001–14. *Journal of Physical Oceanography*, *45*(1), 3–32. https://doi.org/10.1175/JPO-D-14-0044.1

Graly, J., Harrington, J., & Humphrey, N. (2017). Combined diurnal variations of discharge and hydrochemistry of the Isunnguata Sermia outlet, Greenland Ice Sheet. *The Cryosphere*, *11*(3), 1131–1140. https://doi.org/10.5194/tc-11-1131-2017

Grasshoff, K., Ehrhardt, M., & Kremling, K. (1983). In K. Grasshoff, M. Ehrhardt, & K. Kremling (Eds.) *Methods of seawater analysis* (2nd ed.). Verlag Chemie.

Halbach, L., Vihtakari, M., Duarte, P., Everett, A., Granskog, M. A., Hop, H., et al. (2019). Tidewater glaciers and bedrock characteristics control the phytoplankton growth environment in a Fjord in the Arctic. *Frontiers in Marine Science*, *6*. https://doi.org/10.3389/fmars.2019.00254

Hansen, H. P., & Koroleff, F. (1999). Determination of nutrients. In K. Grasshoff, K. Kremling, & M. Ehrhardt (Eds.), *Methods of seawater analysis* (pp. 159–228). Wiley-VCH Verlag GmbH.

Hatton, J. E., Hendry, K. R., Hawkings, J. R., Wadham, J. L., Kohler, T. J., Stibal, M., et al. (2019). Investigation of subglacial weathering under the Greenland Ice Sheet using silicon isotopes. *Geochimica et Cosmochimica Acta*, *247*, 191–206. https://doi.org/10.1016/j.gca.2018.12.033

Hatton, J. E., Ng, H. C., Meire, L., Woodward, E. M. S., Leng, M. J., Coath, C. D., et al. (2023). Silicon isotopes highlight the role of glaciated fjords in modifying coastal waters. *Journal of Geophysical Research: Biogeosciences*, *128*(7), e2022JG007242. https://doi.org/10.1029/2022JG007242

Hawkings, J. R., Wadham, J. L., Benning, L. G., Hendry, K. R., Tranter, M., Tedstone, A., et al. (2017). Ice sheets as a missing source of silica to the polar oceans. *Nature Communications*, *8*(1), 14198. https://doi.org/10.1038/ncomms14198

Holding, J. M., Markager, S., Juul-Pedersen, T., Paulsen, M. L., Møller, E. F., Meire, L., & Sejr, M. K. (2019). Seasonal and spatial patterns of primary production in a high-latitude fjord affected by Greenland Ice Sheet run-off. *Biogeosciences*, *16*(19), 3777–3792. https://doi.org/10.5194/bg-16-3777-2019

Hopwood, M. J., Carroll, D., Browning, T. J., Meire, L., Mortensen, J., Krisch, S., & Achterberg, E. P. (2018). Non-linear response of summertime marine productivity to increased meltwater discharge around Greenland. *Nature Communications*, *9*(1), 3256. https://doi.org/10.1038/s41467-018-05488-8

Hopwood, M. J., Carroll, D., Dunse, T., Hodson, A., Holding, J. M., Iriarte, J. L., et al. (2020). Review article: How does glacier discharge affect marine biogeochemistry and primary production in the Arctic? *The Cryosphere*, *14*(4), 1347–1383. https://doi.org/10.5194/tc-14-1347-2020

Inall, M. E., & Gillibrand, P. A. (2010). The physics of mid-latitude fjords: A review. *Geological Society, London, Special Publications*, *344*(1), 17–33. https://doi.org/10.1144/SP344.3

Jenkins, A. (2011). Convection-driven melting near the grounding lines of ice shelves and tidewater glaciers. *Journal of Physical Oceanography*, *41*(12), 2279–2294. https://doi.org/10.1175/JPO-D-11-03.1

Jørgensen, B. B., Laufer, K., Michaud, A. B., & Wehrmann, L. M. (2021). Biogeochemistry and microbiology of high Arctic marine sediment ecosystems—Case study of Svalbard fjords. *Limnology & Oceanography*, *66*(S1), S273–S292. https://doi.org/10.1002/lno.11551

Juul-Pedersen, T., Arendt, K. E., Mortensen, J., Blicher, M. E., Søgaard, D., & Rysgaard, S. (2015). Seasonal and interannual phytoplankton production in a sub-Arctic tidewater outlet glacier fjord, SW Greenland. *Marine Ecology Progress Series*, *524*, 27–38. https://doi.org/10.3354/meps11174

Kanna, N., Sugiyama, S., Ando, T., Wang, Y., Sakuragi, Y., Hazumi, T., et al. (2022). Meltwater discharge from marine-terminating glaciers drives biogeochemical conditions in a Greenlandic fjord. *Global Biogeochemical Cycles*, *36*(11), e2022GB007411. https://doi.org/10.1029/2022GB007411

Kanna, N., Sugiyama, S., Ohashi, Y., Sakakibara, D., Fukamachi, Y., & Nomura, D. (2018). Upwelling of macronutrients and dissolved inorganic carbon by a subglacial freshwater driven plume in Bowdoin Fjord, northwestern Greenland. *Journal of Geophysical Research: Biogeosciences*, *123*(5), 1666–1682. https://doi.org/10.1029/2017JG004248

Kilpatrick, K. A., Podestá, G., Walsh, S., Williams, E., Halliwell, V., Szczodrak, M., et al. (2015). A decade of sea surface temperature from MODIS. *Remote Sensing of Environment*, *165*, 27–41. https://doi.org/10.1016/j.rse.2015.04.023

Krause, J., Carroll, D., Höfer, J., Donaire, J., Achterberg, E. P., Alarcón, E., et al. (2024). The macronutrient and micronutrient (iron and manganese) content of icebergs. *The Cryosphere*, *18*(12), 5735–5752. https://doi.org/10.5194/tc-18-5735-2024

Krause, J., Hopwood, M. J., Höfer, J., Krisch, S., Achterberg, E. P., Alarcón, E., et al. (2021). Trace element (Fe, Co, Ni and Cu) dynamics across the salinity gradient in arctic and Antarctic Glacier Fjords. *Frontiers in Earth Science*, *9*, 878. https://doi.org/10.3389/feart.2021.725279

Krause, J. W., Duarte, C. M., Marquez, I. A., Assmy, P., Fernández-Méndez, M., Wiedmann, I., et al. (2018). Biogenic silica production and diatom dynamics in the Svalbard region during spring. *Biogeosciences*, *15*(21), 6503–6517. https://doi.org/10.5194/bg-15-6503-2018

Krause, J. W., Schulz, I. K., Rowe, K. A., Dobbins, W., Winding, M. H. S., Sejr, M. K., et al. (2019). Silicic acid limitation drives bloom termination and potential carbon sequestration in an Arctic bloom. *Scientific Reports*, *9*(1), 8149. https://doi.org/10.1038/s41598-019-44587-4

Krawczyk, D. W., Arendt, K. E., Juul-Pedersen, T., Sejr, M. K., Blicher, M. E., & Jakobsen, H. H. (2015). Spatial and temporal distribution of planktonic protists in the East Greenland fjord and offshore waters. *Marine Ecology Progress Series*, *538*, 99–116. https://doi.org/10.3354/meps11439

Krawczyk, D. W., Meire, L., Lopes, C., Juul-Pedersen, T., Mortensen, J., Li, C. L., & Krogh, T. (2018). Seasonal succession, distribution, and diversity of planktonic protists in relation to hydrography of the Godthåbsfjord system (SW Greenland). *Polar Biology*, *41*(10), 2033–2052. https://doi.org/10.1007/s00300-018-2343-0

Krawczyk, D. W., Witkowski, A., Juul-Pedersen, T., Arendt, K. E., Mortensen, J., & Rysgaard, S. (2015). Microplankton succession in a SW Greenland tidewater glacial fjord influenced by coastal inflows and run-off from the Greenland Ice Sheet. *Polar Biology*, *38*(9), 1515–1533. https://doi.org/10.1007/s00300-015-1715-y

Krawczyk, D. W., Witkowski, A., Waniek, J. J., Wroniecki, M., & Harff, J. (2014). Description of diatoms from the Southwest to West Greenland coastal and open marine waters. *Polar Biology*, *37*(11), 1589–1606. https://doi.org/10.1007/s00300-014-1546-2

Krisch, S., Hopwood, M. J., Schaffer, J., Al-Hashem, A., Höfer, J., Rutgers van der Loeff, M. M., et al. (2021). The 79°N Glacier cavity modulates subglacial iron export to the NE Greenland Shelf. *Nature Communications*, *12*(1), 3030. https://doi.org/10.1038/s41467-021-23093-0

Lund-Hansen, L. C., Andersen, T. J., Nielsen, M. H., & Pejrup, M. (2010). Suspended matter, Chl-a, CDOM, grain sizes, and optical properties in the Arctic Fjord-type estuary, Kangerlussuaq, West Greenland during summer. *Estuaries and Coasts*, *33*(6), 1442–1451. https://doi.org/10.1007/s12237-010-9300-7

Lund-Hansen, L. C., Hawes, I., Holtegaard Nielsen, M., Dahllöf, I., & Sorrell, B. K. (2018). Summer meltwater and spring sea ice primary production, light climate and nutrients in an Arctic estuary, Kangerlussuaq, west Greenland. *Arctic Antarctic and Alpine Research*, *50*(1), S100025. https://doi.org/10.1080/15230430.2017.1414468

Luostarinen, T., Ribeiro, S., Weckström, K., Sejr, M., Meire, L., Tallberg, P., & Heikkilä, M. (2020). An annual cycle of diatom succession in two contrasting Greenlandic fjords: From simple sea-ice indicators to varied seasonal strategists. *Marine Micropaleontology*, *158*, 101873. https://doi.org/10.1016/j.marmicro.2020.101873

Mankoff, K. D., Noël, B., Fettweis, X., Ahlstrøm, A. P., Colgan, W., Kondo, K., et al. (2020b). Greenland liquid water discharge from 1958 through 2019. *Earth System Science Data*, *12*(4), 2811–2841. https://doi.org/10.5194/essd-12-2811-2020

Mankoff, K. D., Solgaard, A., Colgan, W., Ahlstrøm, A. P., Khan, S. A., & Fausto, R. S. (2020a). Greenland Ice Sheet solid ice discharge from 1986 through March 2020. *Earth System Science Data*, *12*(2), 1367–1383. https://doi.org/10.5194/essd-12-1367-2020

Martín, J., Tremblay, J. E., Gagnon, J., Tremblay, G., Lapoussière, A., Jose, C., et al. (2010). Prevalence, structure and properties of subsurface chlorophyll maxima in Canadian Arctic waters. *Marine Ecology Progress Series*, *412*, 69–84. https://doi.org/10.3354/meps08666

Martin, J. B., Pain, A. J., Martin, E. E., Rahman, S., & Ackerman, P. (2020). Comparisons of nutrients exported from Greenlandic glacial and deglaciated watersheds. *Global Biogeochemical Cycles*, *34*(12), e2020GB006661. https://doi.org/10.1029/2020GB006661

Meire, L., Meire, P., Struyf, E., Krawczyk, D. W., Arendt, K. E., Yde, J. C., et al. (2016). High export of dissolved silica from the Greenland Ice Sheet. *Geophysical Research Letters*, *43*(17), 9173–9182. https://doi.org/10.1002/2016GL070191

Meire, L., Mortensen, J., Meire, P., Juul-Pedersen, T., Sejr, M. K., Rysgaard, S., et al. (2017). Marine-terminating glaciers sustain high productivity in Greenland fjords. *Global Change Biology*, *23*(12), 5344–5357. https://doi.org/10.1111/gcb.13801

Møller, E. F., Christensen, A., Larsen, J., Mankoff, K. D., Ribergaard, M. H., Sejr, M., et al. (2023). The sensitivity of primary productivity in Disko Bay, a coastal Arctic ecosystem, to changes in freshwater discharge and sea ice cover. *Ocean Science*, *19*(2), 403–420. https://doi.org/10.5194/os-19-403-2023

Mortensen, J., Rysgaard, S., Arendt, K. E., Juul-Pedersen, T., Søgaard, D. H., Bendtsen, J., & Meire, L. (2018). Local coastal water masses control heat levels in a West Greenland tidewater outlet Glacier Fjord. *Journal of Geophysical Research: Oceans*, *123*(11), 8068–8083. https://doi.org/10.1029/2018JC014549

Mortensen, J., Rysgaard, S., Bendtsen, J., Lennert, K., Kanzow, T., Lund, H., & Meire, L. (2020). Subglacial discharge and its down-fjord transformation in west Greenland fjords with an ice Mélange. *Journal of Geophysical Research: Oceans*, *125*(9), e2020JC016301. https://doi.org/10.1029/2020JC016301

Mugford, R. I., & Dowdeswell, J. A. (2011). Modeling glacial meltwater plume dynamics and sedimentation in high-latitude fjords. *Journal of Geophysical Research*, *116*(F1). https://doi.org/10.1029/2010JF001735

Murray, C., Markager, S., Stedmon, C. A., Juul-Pedersen, T., Sejr, M. K., & Bruhn, A. (2015). The influence of glacial melt water on bio-optical properties in two contrasting Greenlandic fjords. *Estuarine, Coastal and Shelf Science*, *163*(PB), 72–83. https://doi.org/10.1016/j.ecss.2015.05.041

Ng, H. C., Cassarino, L., Pickering, R. A., Woodward, E. M. S., Hammond, S. J., & Hendry, K. R. (2020). Sediment efflux of silicon on the Greenland margin and implications for the marine silicon cycle. *Earth and Planetary Science Letters*, *529*, 115877. https://doi.org/10.1016/j.epsl.2019.115877

Ng, H. C., Hendry, K. R., Ward, R., Woodward, E. M. S., Leng, M. J., Pickering, R. A., & Krause, J. W. (2024). Detrital input sustains diatom production off a glaciated Arctic Coast. *Geophysical Research Letters*, *51*(12), e2024GL108324. https://doi.org/10.1029/2024GL108324

Oliver, H., Castelao, R. M., Wang, C., & Yager, P. L. (2020). Meltwater-enhanced nutrient export from Greenland's Glacial Fjords: A sensitivity analysis. *Journal of Geophysical Research: Oceans*, *125*(7), e2020JC016185. https://doi.org/10.1029/2020JC016185

Oliver, H., Slater, D., Carroll, D., Wood, M., Morlighem, M., & Hopwood, M. J. (2023). Greenland subglacial discharge as a driver of hotspots of increasing coastal chlorophyll since the early 2000s. *Geophysical Research Letters*, *50*(10), e2022GL102689. https://doi.org/10.1029/2022GL102689

Randelhoff, A., Holding, J., Janout, M., Sejr, M. K., Babin, M., Tremblay, J. É., & Alkire, M. B. (2020). Pan-Arctic ocean primary production constrained by turbulent nitrate fluxes. *Frontiers in Marine Science*, *7*. https://doi.org/10.3389/fmars.2020.00150

Sathyendranath, S., Brewin, R. J. W., Brockmann, C., Brotas, V., Calton, B., Chuprin, A., et al. (2019). An ocean-colour time series for use in climate studies: The experience of the ocean-colour climate change initiative (OC-CCI). *Sensors*, *19*, 4285. https://doi.org/10.3390/s19194285

Schumann, K., Völker, D., & Weinrebe, W. R. (2012). Acoustic mapping of the Ilulissat Ice Fjord mouth, West Greenland. *Quaternary Science Reviews*, *40*, 78–88. https://doi.org/10.1016/j.quascirev.2012.02.016

Seifert, M., Hoppema, M., Burau, C., Friedrichs, A., Geuer, J. K., John, U., et al. (2019). Influence of glacial meltwater on summer biogeochemical cycles in Scoresby Sund, East Greenland. *Frontiers in Marine Science*, *6*. https://doi.org/10.3389/fmars.2019.00412

Sejr, M. K., Bruhn, A., Dalsgaard, T., Juul-Pedersen, T., Stedmon, C. A., Blicher, M., et al. (2022). Glacial meltwater determines the balance between autotrophic and heterotrophic processes in a Greenland fjord. *Proceedings of the National Academy of Sciences*, *119*(52), e2207024119. https://doi.org/10.1073/pnas.2207024119

Slater, D. A., Carroll, D., Oliver, H., Hopwood, M. J., Straneo, F., Wood, M., et al. (2022). Characteristic depths, fluxes, and timescales for Greenland's Tidewater glacier fjords from subglacial discharge-driven upwelling during summer. *Geophysical Research Letters*, *49*(10), e2021GL097081. https://doi.org/10.1029/2021GL097081

Smith, L. M., & Andrews, J. T. (2000). Sediment characteristics in iceberg dominated fjords, Kangerlussuaq region, East Greenland. *Sedimentary Geology*, *130*(1), 11–25. https://doi.org/10.1016/S0037-0738(99)00088-3

Stimmler, P., Goeckede, M., Elberling, B., Natali, S., Kuhry, P., Perron, N., et al. (2023). Pan-Arctic soil element bioavailability estimations. *Earth System Science Data*, *15*(3), 1059–1075. https://doi.org/10.5194/essd-15-1059-2023

Straneo, F., & Cenedese, C. (2015). The dynamics of Greenland's glacial fjords and their role in climate. *Annual Review of Marine Science*, *7*(1), 89–112. https://doi.org/10.1146/annurev-marine-010213-135133

Stuart-Lee, A. E., Mortensen, J., Juul-Pedersen, T., Middelburg, J. J., Soetaert, K., Hopwood, M. J., et al. (2023). Influence of glacier type on bloom phenology in two Southwest Greenland fjords. *Estuarine, Coastal and Shelf Science*, *284*, 108271. https://doi.org/10.1016/j.ecss.2023.108271

Stuart-Lee, A. E., Mortensen, J., van der Kaaden, A.-S., & Meire, L. (2021). Seasonal hydrography of Ameralik: A southwest Greenland fjord impacted by a land-terminating glacier. *Journal of Geophysical Research: Oceans*, *126*(12), e2021JC017552. https://doi.org/10.1029/2021JC017552

Syvitski, J. P. M., Andrews, J. T., & Dowdeswell, J. A. (1996). Sediment deposition in an iceberg-dominated glacimarine environment, East Greenland: Basin fill implications. *Global and Planetary Change*, *12*(1), 251–270. https://doi.org/10.1016/0921-8181(95)00023-2

Tesdal, J.-E., Ducklow, H. W., Goes, J. I., & Yashayaev, I. (2022). Recent nutrient enrichment and high biological productivity in the Labrador Sea is tied to enhanced winter convection. *Progress in Oceanography*, *102848*, 102848. https://doi.org/10.1016/j.pocean.2022.102848

The Greenland Ecosystem Monitoring (GEM) Database. [Dataset]. Retrieved from https://g-e-m.dk

Torres, R., Silva, N., Reid, B., & Frangopulos, M. (2014). Silicic acid enrichment of subantarctic surface water from continental inputs along the Patagonian archipelago interior sea (41–56°S). *Progress in Oceanography*, *129*(A), 50–61. https://doi.org/10.1016/j.pocean.2014.09.008

Tréguer, P. J., & De La Rocha, C. L. (2013). The world ocean silica cycle. *Annual Review of Marine Science*, *5*(1), 477–501. https://doi.org/10.1146/annurev-marine-121211-172346

Tréguer, P. J., Sutton, J. N., Brzezinski, M., Charette, M. A., Devries, T., Dutkiewicz, S., et al. (2021). Reviews and syntheses: The biogeochemical cycle of silicon in the modern ocean. *Biogeosciences*, *18*(4), 1269–1289. https://doi.org/10.5194/bg-18-1269-2021

Yde, J. C., Knudsen, N. T., Hasholt, B., & Mikkelsen, A. B. (2014). Meltwater chemistry and solute export from a Greenland Ice Sheet catchment, Watson River, West Greenland. *Journal of Hydrology*, *519*, 2165–2179. https://doi.org/10.1016/j.jhydrol.2014.10.018

Yde, J. C., Tvis Knudsen, N., & Nielsen, O. B. (2005). Glacier hydrochemistry, solute provenance, and chemical denudation at a surge-type glacier in Kuannersuit Kuussuat, Disko Island, West Greenland. *Journal of Hydrology*, *300*(1), 172–187. https://doi.org/10.1016/j.jhydrol.2004.06.008

Zajączkowski, M., & Włodarska-Kowalczuk, M. (2007). Dynamic sedimentary environments of an Arctic glacier-fed river estuary (Adventfjorden, Svalbard). I. Flux, deposition, and sediment dynamics. *Estuarine, Coastal and Shelf Science*, *74*(1), 285–296. https://doi.org/10.1016/j.ecss.2007.04.015

Zhu, X., Hopwood, M. J., Laufer-Meiser, K., & Achterberg, E. P. (2024). Incubation experiments characterize turbid glacier plumes as a major source of Mn and Co, and a minor source of Fe and Si, to seawater. *Global Biogeochemical Cycles*, *38*(10), e2024GB008144. https://doi.org/10.1029/2024GB008144